iScience

Article

Post-testicular spermatozoa of a marine teleost can conduct *de novo* cytoplasmic and mitochondrial translation

Graphical abstract

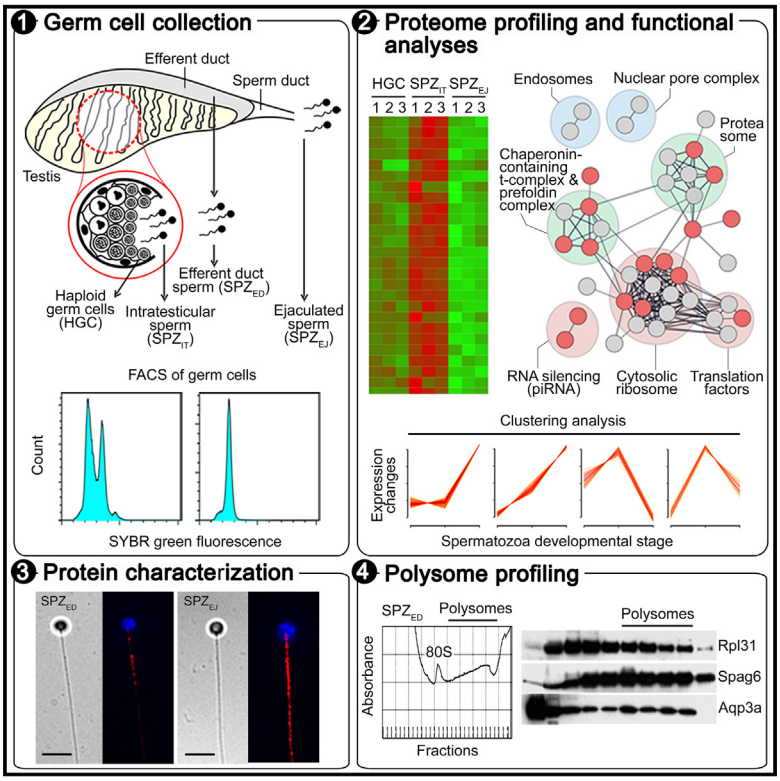

Highlights

- Maturing spermatozoa sequentially accumulate proteins for translation and motility
- Increased fertility competence requires active translation in the post-testicular sperm
- Cytosolic and mitochondrial ribosomes drive the *de novo* protein synthesis

Authors

Júlia Castro-Arnau, François Chauvigné, Asier González, Roderick Nigel Finn, Montserrat Carrascal, Joan Cerdà

Correspondence

jcerda@icm.csic.es

In brief

Piscine reproduction; Biological sciences; Zoology

Castro-Arnau et al., 2025, iScience *28*, 111537
January 17, 2025 © 2024 The Author(s). Published by Elsevier Inc.
https://doi.org/10.1016/j.isci.2024.111537

CellPress

iScience

CellPress
OPEN ACCESS

Article

Post-testicular spermatozoa of a marine teleost can conduct *de novo* cytoplasmic and mitochondrial translation

Júlia Castro-Arnau,[1,2,5] François Chauvigné,[1,2] Asier González,[2] Roderick Nigel Finn,[1,2,3] Montserrat Carrascal,[4] and Joan Cerdà[1,2,6,*]

[1]Institute of Marine Sciences, Spanish National Research Council (CSIC), 08003 Barcelona, Spain
[2]Institute of Biotechnology and Biomedicine, Universitat Autònoma de Barcelona, Bellaterra, 08193 Barcelona, Spain
[3]Department of Biological Sciences, University of Bergen, 5020 Bergen, Norway
[4]Biological and Environmental Proteomics Group, Institute of Biomedical Research of Barcelona, Spanish National Research Council (IIBB-CSIC/IDIBAPS), 08036 Barcelona, Spain
[5]Present address: Department of Cell Biology & Physiology, Washington University School of Medicine in St. Louis, St. Louis, MO 63110, USA
[6]Lead contact
*Correspondence: jcerda@icm.csic.es
https://doi.org/10.1016/j.isci.2024.111537

SUMMARY

Translational silence of spermatozoa has long been considered the norm in animals. However, studies in mammals have shown that the mitochondrial ribosomal machinery is selectively activated during capacitation in the female reproductive tract, while cytosolic ribosomes remain inactive. Here, using quantitative proteomics in a piscine model species, we show that proteins involved in mRNA processing and cytoplasmic translation are predominantly accumulated in immature spermatozoa within the extratesticular excurrent ducts, while those related to flagellar motility are enriched in ejaculated (mature) sperm. Based upon *in vitro* incubation of isolated spermatozoa, motility assays and polysome profiling, we further show that 80S cytoplasmic and 55S mitochondrial ribosomes are actively involved in the translation of motility- and osmoadaptation-related proteins. These findings thus reveal that post-testicular piscine spermatozoa can maintain *de novo* protein synthesis through both mitochondrial and cytoplasmic ribosomal activity, which is necessary for the acquisition of full sperm function.

INTRODUCTION

Vertebrate spermatogenesis proceeds in a multistage process from mitotic expansion of spermatogonial stem cells to form primary spermatocytes (SPC), which through two meiotic divisions become haploid spermatids (SPD) that differentiate into the highly polarized spermatozoa (spermiogenesis) retaining a recombined haploid genome.[1,2] Spermiogenesis encompasses substantial remodeling of the cytoplasmic and nuclear architecture, including DNA compaction, elimination of cellular material, flagellum formation, and the rearrangement of cellular organelles along the spermatozoon cytoplasm.[1] At the culmination of this process, however, the fully differentiated spermatozoa are typically not capable of fertilizing the egg.[3,4] They require a maturational phase, which confers the physiological ability to move, recognize, and penetrate the egg.[3,4] In most vertebrates, this process occurs during sperm storage and transit through the extratesticular excurrent ducts (ETDs) and tubular systems that emanate from the testis, which in amniotes form the epididymis.[3,5]

In mammals, studies using mass spectrometry-based proteomics to systemically investigate protein abundances and modifications in the testis and sperm have advanced our knowledge of the molecular mechanisms of spermatogenesis.[6] This includes how the epididymal maturation is accompanied by substantial remodeling of the sperm proteome, including the accumulation of several proteins associated with sperm motility and fertility.[7–9] In addition to the release of epididymosomes (small membrane bound extracellular vesicles) from the epididymal epithelium,[10] which deliver somatic protein cargo to the maturing spermatozoa,[8] an increasing number of studies suggest that *de novo* translation also occurs in the ejaculated spermatozoa during exposure to the female genital fluids leading to capacitation and fertility competence.[11–17] To date, however, only mitochondrial translation has been demonstrated, while cytoplasmic ribosomal activity remains silent, although the mechanism by which nuclear mRNAs are transported to the mitochondria remains to be elucidated.[12,14,15,17]

In oviparous vertebrates with external fertilization, such as teleost fish, spermatozoa remain quiescent in the testes and ETDs after spermiogenesis, and the initiation of motility is triggered by the hypo- or hyperosmotic aquatic environment into which the sperm are ejaculated.[4] In these species, the ETDs are considered to be involved in the formation of the seminal

This is an open access article under the CC BY-NC-ND license (http://creativecommons.org/licenses/by-nc-nd/4.0/).

fluid, the control of its pH and ion composition, and the nutrition of spermatozoa to maintain their viability prior to ejaculation.[4,18] However, the molecular mechanisms that are required for the acquisition of sperm motility competence during passage through the ETDs are completely unknown. Proteomic studies during teleost spermatogenesis have mainly been conducted on the whole testis,[19–22] seminal fluid,[23,24] or on ejaculated sperm to evaluate changes in the proteome upon motility activation and maintenance, or after short- or long-term storage.[24–28] In contrast, few studies have identified protein changes concurrent with the differentiation of spermatozoa and the acquisition of their fertilization capacity.[21,29] There is thus a distinct lack of information in fishes on the gametic proteome changes during intratesticular spermiogenesis and ETD maturation, and whether their post-testicular spermatozoa are translationally competent.

To address this knowledge gap, in the present study we conducted liquid chromatography-tandem mass spectrometry (LC-MS/MS)-based quantitative proteomics in the marine teleost gilthead seabream (*Sparus aurata*) to identify changes in the sperm proteome associated with their intratesticular differentiation and subsequent maturation in the ETDs. In addition, using immunolocalization and immunoblotting of ribosomal proteins, together with *in vitro* experiments, sperm motility assays and sperm polysome profiling, we provide evidence for both cytoplasmic and mitochondrial translation in teleost spermatozoa during their post-testicular maturation in the ETDs.

RESULTS

Global proteomic analysis of seabream spermatozoa

In the seabream, as in other teleosts, the testes are usually elongated paired organs attached to the dorsal body wall, which are located ventral to the swim bladder and dorsal to the intestine[30] (Figure 1A). The ETDs are formed by the efferent duct (ED), that arises from the dorsal surface of each elongated testis, and the unpaired spermatic duct (SD) segment, which connects both EDs and opens into the urogenital papilla (Figure 1A). Spermatogenesis occurs in the seminiferous tubules within the testis, where spermatogonia form primary diploid spermatocytes type I (SPCI), which subsequently undergo meiosis I to form haploid secondary SPC type II (SPCII). These secondary SPC further divide through meiosis II, producing haploid spermatids (SPD), which differentiate into spermatozoa that are released into the lumen of the seminiferous tubules (here termed SPZ_{IT}), and are eventually transported to the ED and SD for ejaculation (Figure 1A).

To investigate changes in the whole proteome during spermatozoon differentiation and maturation, we isolated highly enriched populations of haploid germ cells (HGC), containing SPCII and SPD, and SPZ_{IT} by fluorescence-activated cell sorting (FACS) of testicular extracts as described previously.[31] Flow cytometry of the whole mature testis showed the proportion of HGC and SPZ_{IT} to be around 42% and 58%, respectively (Figure 1B). The ejaculated spermatozoa (SPZ_{EJ}) were collected by manual stripping of naturally spermiating males, with subsequent flow cytometry showing that 99% of cells in the ejaculated semen corresponded to mature spermatozoa (Figure 1B). The kinematic parameters of the spermatozoa were determined by computer-assisted sperm analysis (CASA) at ~5 s post activation in seawater (Figure 1C). The results showed that the percentage of total motile and progressive SPZ_{IT} (%MOT and % PROG, respectively), as well as the curvilinear velocity (VCL), were lower with respect to the SPZ_{EJ} (Figure 1C). These data therefore indicate that SPZ_{IT} can be classified as immature gametes, which are yet to acquire full motility potential.

The different HGC, SPZ_{IT} and SPZ_{EJ} cell populations were then subjected to trypsin digestion, tandem mass tag (TMT) labeling and MS analysis. For this analysis, we used three biological replicates per each population, each replicate being a pool of cells collected from five different males. Mass spectrometry-driven proteomics analysis identified a total of 502 unique proteins with high confidence (1% FDR) and at least two identified peptide-spectrum matches (PSMs) (Table S1). Initial interrogation of this global proteome on the basis of shared functional classification using the QuickGO browser[32] and Panther classification system[33] returned dominant terms of "minus-end-directed microtubule motor activity" (GO identifier: 0008569), "dynein light intermediate chain binding" and "dynein intermediate chain binding" (GO identifiers: 0051959 and 0045505, respectively), "unfolded protein binding" (GO identifier: 0051082) and "oxidoreductase activity, acting on a sulfur group of donors" (GO identifier: 0016667) among the top 15 GO molecular function categories when ranked on the basis of their fold enrichment (Figure 1D and Table S2). Similarly, in terms of GO biological process categories, notable enrichment was identified in the broad term of "epithelial cilium movement involved in extracellular fluid movement" (GO identifier: 0003351), "regulation of cilium movement" (GO identifier: 0003352), "cilium movement involved in cell motility" (GO identifier: 0060294), "flagellated sperm motility" (GO identifier: 0030317), and "cellular respiration" (GO identifier: 0045333) (Figure 1E and Table S2). Interestingly, we also found some enrichment for the GO biological process category "translation" (GO identifier: 0006412), as well as notable representation of the GO cellular component term "protein folding chaperone complex" (GO identifier: 0101031) (Figure 1F and Table S2), which is usually active during or immediately after completion of translation. Other dominant GO cellular component categories included "fatty acid beta-oxidation multienzyme complex" (GO identifier: 0036125), "peptidase complex" (GO identifier: 1905368), "ATPase complex" (GO identifier: 1904949) and "polysome" (GO identifier: 0005844) (Figure 1F and Table S2).

Relative quantification of differential protein accumulation during the differentiation and maturation of spermatozoa

To better understand how the proteome changes with germ cell development, principal component analysis (PCA) was performed based on the fluorescent protein intensity. PCA analysis revealed a high level of concordance among the biological replicates comprising each experimental group (Figure S1). Notably, this analysis also showed that each subpopulation was well separated, suggesting that the developmental stage has a large effect on the pattern of protein expression. In particular, HGC replicates were found to reside directly opposed to those of

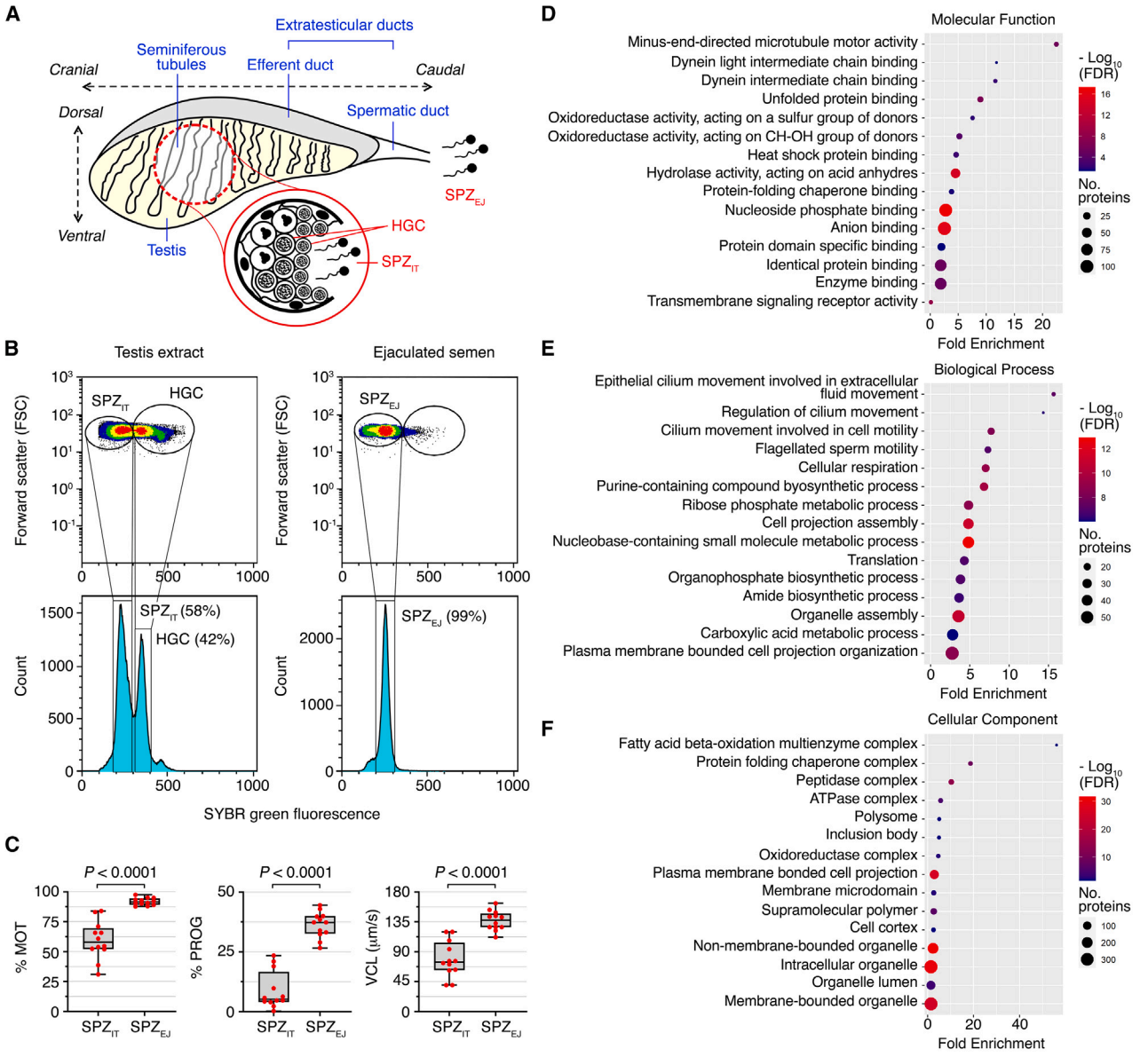

Figure 1. Global proteomic analysis of seabream HCG, SPZ_{IT} and SPZ_{EJ}

(A) Schematic representation of the seabream testis showing one testicular lobule and extratesticular excurrent ducts (ETDs), including the efferent duct (ED) and spermatic duct (SD), and the developing germ cells within the testicular seminiferous tubules. HGC, haploid germ cells; SPZ_{IT}, intratesticular spermatozoa; SPZ_{EJ}, ejaculated spermatozoa.

(B) Representative flow cytometry plots of the cell populations in the whole testis and ejaculated semen. The DNA of the cells were stained with SYBR Green I fluorescent dye and the DNA content distribution in HGC and SPZ_{IT} in the testis extract, and in SPZ_{EJ} in the ejaculates, is shown as scatterplots (upper panels) and histograms (lower panels). In the testis, the different subpopulations of HGC, corresponding to a mix of type II spermatocytes and spermatids, and SPZ_{IT} are shown. In the ejaculates, ~99% of the cells correspond to SPZ_{EJ}.

(C) Percentage of motility (% MOT), progressivity (% PROG) and curvilinear velocity (VCL) of SPZ_{IT} and SPZ_{EJ} determined by CASA at ~5 s post activation in seawater. The data points (red dots) are presented as box and whisker plots/scatter dots with horizontal line (inside box) indicating median and outliers (n = 12 males). Statistical differences were measured by the Student's t test or by the nonparametric Mann Whitney test, and the calculated p-values are indicated in each plot.

(D–F) Gene ontology (GO) enrichment analysis (FDR $\leq$0.05) of all identified and annotated proteins with changing expression across HCG, SPZ_{IT} and SPZ_{EJ}. The plots show the top 15 GO terms for each GO domain, Molecular function (level 3) (D), Biological process (level 5) (E) and Cellular component (level 3) (F), when ranked on the basis of their fold enrichment.

the SPZ_{IT} and SPZ_{EJ} groups, with the principal component 1 (PC1) accounting for ~69% of the observed variance.

We next investigated the protein expression differences between the three HGC, SPZ_{IT} and SPZ_{EJ} groups. To determine which of these expression changes were statistically significant, DanteR analysis[34] was performed from which only proteins having a *p*-value below 0.05 (5% FDR) and fold-change over 1.15 or lower than 0.87 in TMT ion intensity, were regarded as significantly regulated. For *in silico* analysis of protein profiles during spermiogenesis, protein abundance data were initially assessed via volcano plots to visualize trends associated with differentially accumulating proteins. With this analysis, we detected 77 proteins significantly regulated between SPZ_{IT} and HGC, 236 proteins between SPZ_{EJ} and SPZ_{IT}, and 189 proteins between in SPZ_{EJ} versus HGC (Figures 2A–2C; Table S3). To characterize how proteins change their expression from HCG to SPZ_{IT} and SPZ_{ED}, the total identified proteins were further grouped using the VSClust algorithm.[35] This analysis was able to cluster 312 of these proteins into four different protein dynamic profiles, named clusters 1 to 4. Clusters 1 and 2 comprised proteins more accumulated in SPZ_{EJ} (140 and 91 proteins, respectively), whereas clusters 3 and 4 contain proteins more expressed in SPZ_{IT} (51 and 30 proteins, respectively) (Figures 2D–2G and Table S4). The proteins in each cluster were manually classified into functional categories by using GO analysis and the Uniprot database. Almost half of the proteins from cluster 1 were related with cytoskeleton, flagella and cell movement (49%), followed by proteins of metabolism and energy dissipation (10%), signal transduction (8%), transcription and translation proteins (8%) and protein synthesis, folding and turnover (7%) (Figure 2H and Table S5). Proteins involved in metabolism and energy dissipation (25%), and protein synthesis, folding and turnover (25%), were the most abundant in cluster 2, followed by transport (11%) and signal transduction proteins (10%) (Figure 2I and Table S5). In contrast, in cluster 3, more than a half of the proteins were related to transcription and translation (64%), followed by protein synthesis, folding and turnover (14%), cytoskeleton, flagella and cell movement (12%) (Figure 2J and Table S5). Finally, most of the proteins in cluster 4 corresponded to protein synthesis, folding and turnover (43%), transcription and translation (17%), and transport (13%) (Figure 2K and Table S5).

Based on the thresholds of the differentially expressed proteins, we constructed hierarchical clustering heatmaps of proteins significantly accumulated in SPZ_{IT} (from clusters 3 and 4) or SPZ_{EJ} (from clusters 1 and 2). The heatmaps showed that most of the proteins accumulated in SPZ_{IT} are related to transcription and translation, and protein synthesis, folding and turnover (Figure 3A and Table S5). Thus, the highest expressed proteins in SPZ_{IT} were eukaryotic translation elongation factor 1 alpha 1 (Eef1a1), polyadenylate-binding protein 1 (Pabpc1), 40S ribosomal protein S19 (Rps19) and ribosomal protein S13 (Rps13). In contrast, the majority of proteins significantly accumulated in SPZ_{EJ} corresponded to cytoskeleton, flagella and cell movement, followed by signal transduction proteins (Figure 3B and Table S5). The most accumulated proteins were dynein light chain 2 (Dynll2), cilia- and flagella-associated protein 53 (Cfap53) and Ropporin-1 (Ropn1), a protein involved in fibrous sheath integrity and sperm motility.[36]

To further investigate the potential role of the proteins highly accumulated in SPZ_{IT} or SPZ_{EJ}, we built putative protein-protein interaction (PPI) networks of all proteins classified in clusters 3 and 4 or clusters 1 and 2 by using STRING for known PPIs,[37] and further highlight those proteins that were significantly higher expressed in each cell type. For the SPZ_{IT} proteins, a connected network comprising 75 proteins and 142 connections was mapped, in which significantly accumulated proteins were classified into different subclusters based on the STRING network clusters and KEGG pathways, such as chaperonin-containing t-complex and prefolding complex, proteasome, translation factors, cytosolic ribosome and RNA silencing (Piwi-interacting RNA [piRNA]) (Figure 3C). Some other proteins accumulated in SPZ_{IT}, although not significantly, were classified into the endosomes and nuclear pore complex subclusters. In contrast, the PPI network of proteins accumulated in SPZ_{EJ} contained 167 proteins and 101 connections in seven subclusters, but most of the significantly higher expressed proteins were classified into the axoneme assembly and motile cilium, and microtubule motor activity and dynactin complex subclusters (Figure 3D). The other subclusters mapped in the PPI network of SPZ_{EJ} were amino acid metabolism, oxidative phosphorylation (OXPHOS), tricarboxylic acid (TCA) cycle, removal of superoxide radicals and peroxidase, and proteasome, but the accumulated proteins belonging to these subclusters did not show statistically significant differences with respect to the SPZ_{IT}.

Altogether, our data suggest that translation mechanisms and protein synthesis processes may be upregulated during early maturation of SPZ_{IT} following the differentiation from HGC, while proteins involved in flagellar motility seem to be accumulated later, prior to spermatozoon ejaculation.

Validation of differentially accumulated proteins in SPZ_{IT} and SPZ_{EJ}

To confirm the differential accumulation of proteins in SPZ_{IT} or SPZ_{EJ} by the LC-MS/MS analysis, four candidate proteins were selected for targeted validation via immunofluorescence microscopy and semiquantitative immunoblot densitometry. For these experiments, we used SPZ_{IT} and SPZ_{EJ} samples from individual fish (n = 3–4 animals/cell population), differing from those employed for MS analyses. The target proteins were selected based on their high abundance in SPZ_{IT} before experiencing reduced abundance in SPZ_{EJ} (Eef1a1 and Rps13), or vice versa, such as α-tubulin (Tuba) and dynein axonemal intermediate chain 2 (Dnai2), and the availability of commercial antibodies cross-reacting with the seabream proteins. Immunostaining experiments revealed that each of the selected proteins were expressed in the cytoplasm of HGC (SPCII and SPD), except Dnai2, which was only detected in SPCII but not in SPD (Figure 4A). In SPZ_{IT}, the Eef1a1 was distributed around the head and in some regions along the flagellum, while its expression became restricted to the anterior part of the tail in SPZ_{EJ} (Figure 4A). The Rps13 was also expressed in the head and in the anterior region of the flagellum in SPZ_{IT}, but in SPZ_{EJ} the staining was more reduced in the head and was no longer detected in the flagellum (Figure 4A). In contrast, Tuba immunostaining was only present along the entire tail of both SPZ_{IT} and SPZ_{EJ}, the staining being less intense in SPZ_{IT} (Figure 4A).

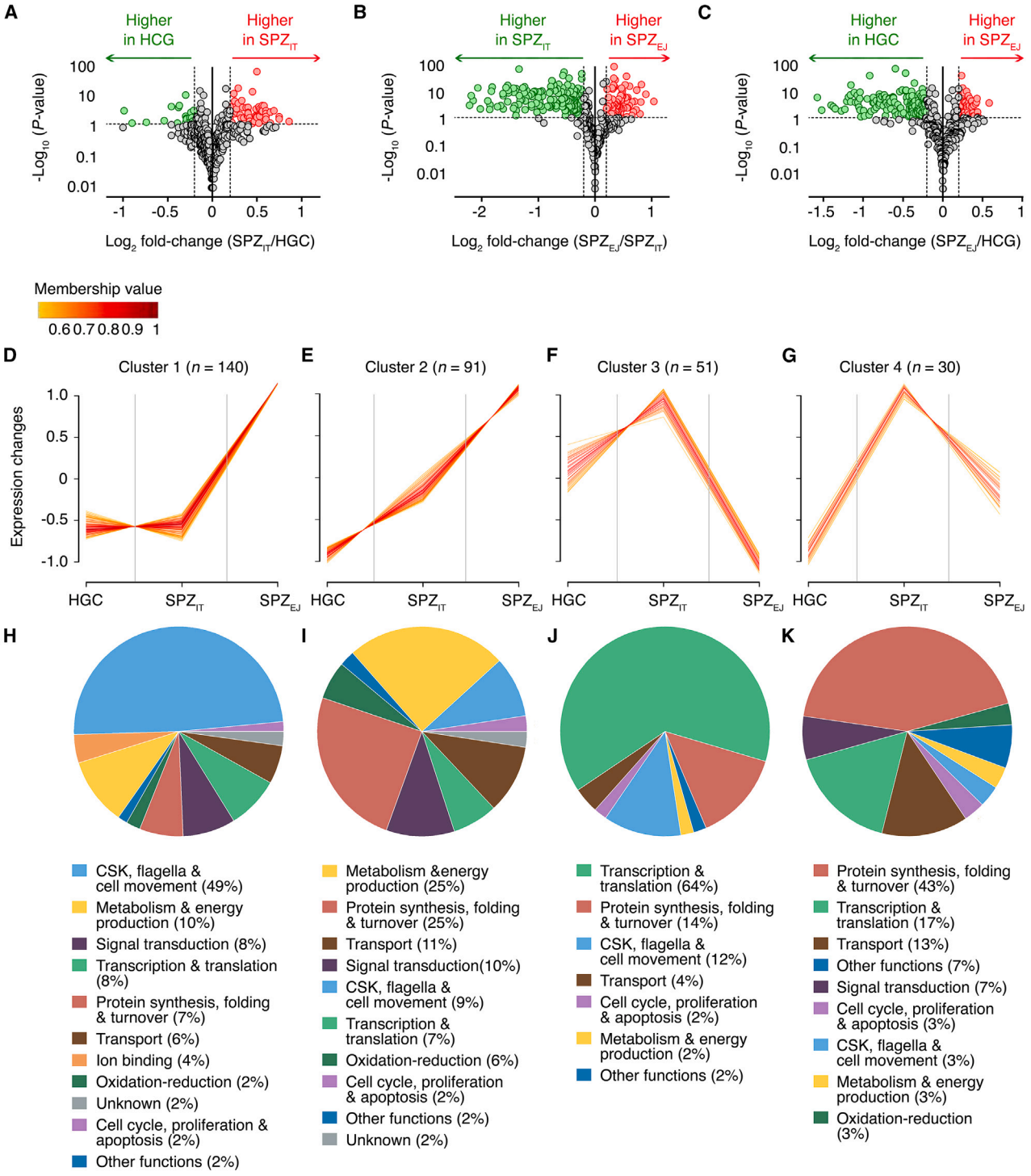

Figure 2. Relative quantification of differential protein accumulation during the differentiation and maturation of spermatozoa

(A–C) Volcano plots depicting the $\log_2$ fold change in expression (x axis) and the negative logarithm of their *p*-value to base 10 (y axis) of proteins that were determined to be significantly differentially accumulated in SPZ_{IT} vs. HGC (A), SPZ_{EJ} vs. SPZ_{IT} (B), and SPZ_{EJ} vs. HGC (C). A threshold of >1.15- or <0.87-fold change ($\log_2$ fold-change of ±0.2) ($p < 0.05$) in TMT ion intensity was established to identify differentially accumulated proteins in SPZ_{IT} and SPZ_{EJ}.

(D–G) Protein dynamic abundance clusters over the three developmental stages obtained with the VSClust algorithm, where the protein abundance is represented by a log-transformed normalized value. Proteins with ≥0.5 membership value are plotted. All the identified proteins were used for this analysis.

(H–K) Pie charts showing the distribution of the functional categories of the proteins within each cluster based on GO analysis and the Uniprot database.

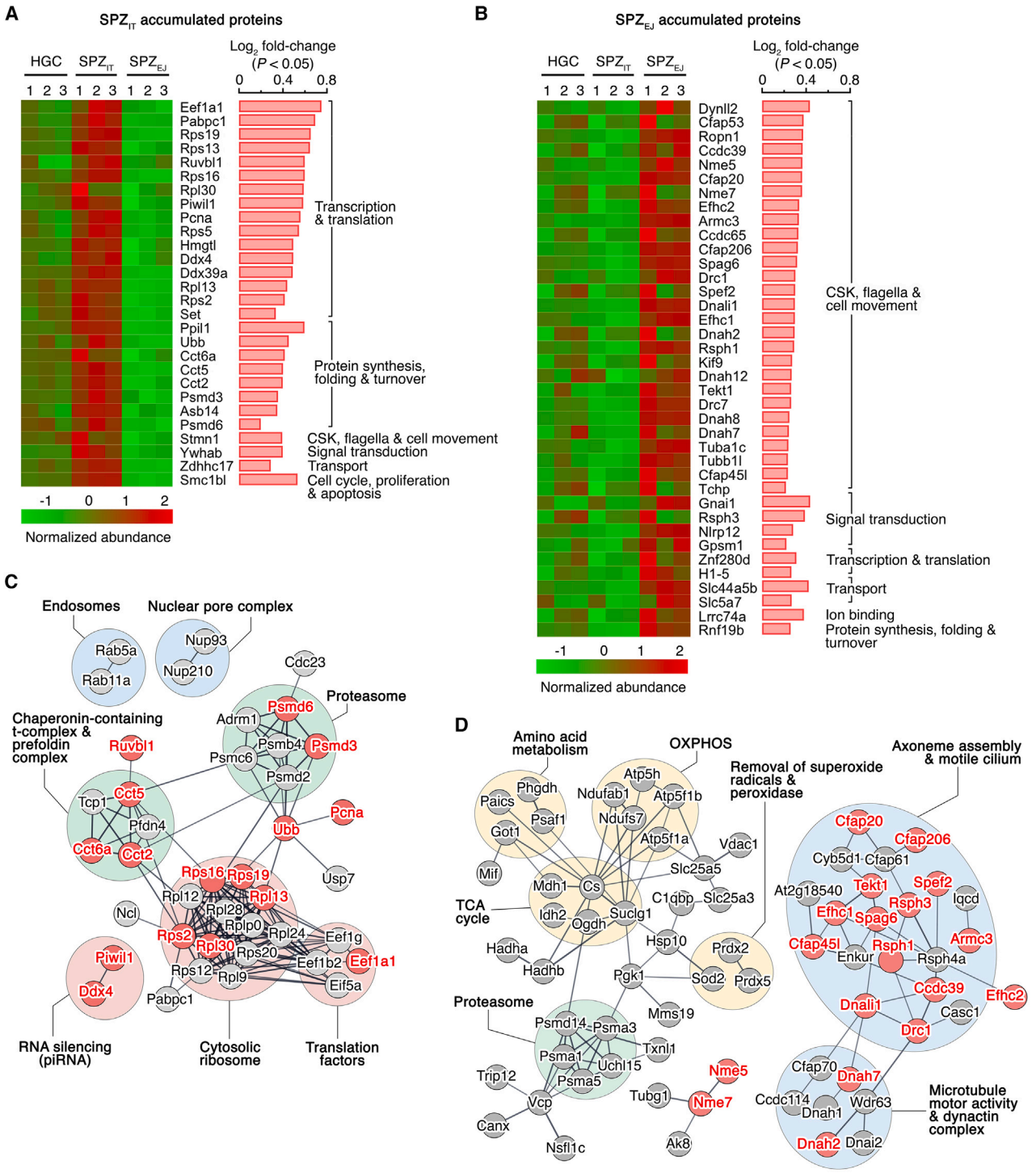

Figure 3. Expression profile and potential interactions of accumulated proteins in SPZ_{IT} and SPZ_{EJ}

(A and B) Hierarchical clustering heatmaps of significantly ($p < 0.05$) accumulated proteins in SPZ_{IT} (A) and SPZ_{EJ} (B) with respect to HGC, included in clusters 3 and 4, and 1 and 2, respectively, shown in Figure 2. The log_2 fold changes and functional categories are represented for each protein.

(C and D) Protein-protein interaction networks of all the proteins within clusters 1 + 2 and 3 + 4 obtained through database searches using STRING with a high confidence interaction score (0.7). Proteins and their interactions are shown as nodes (spheres) and edges (lines), respectively. Proteins were grouped based on STRING network subclusters and KEGG pathways. Nodes in red color indicate significantly accumulated proteins in SPZ_{IT} (C) and SPZ_{EJ} (D). Nodes in gray color indicate not significantly expressed proteins. Abbreviations: OXPHOS, oxidative phosphorylation; TCA, tricarboxylic acid.

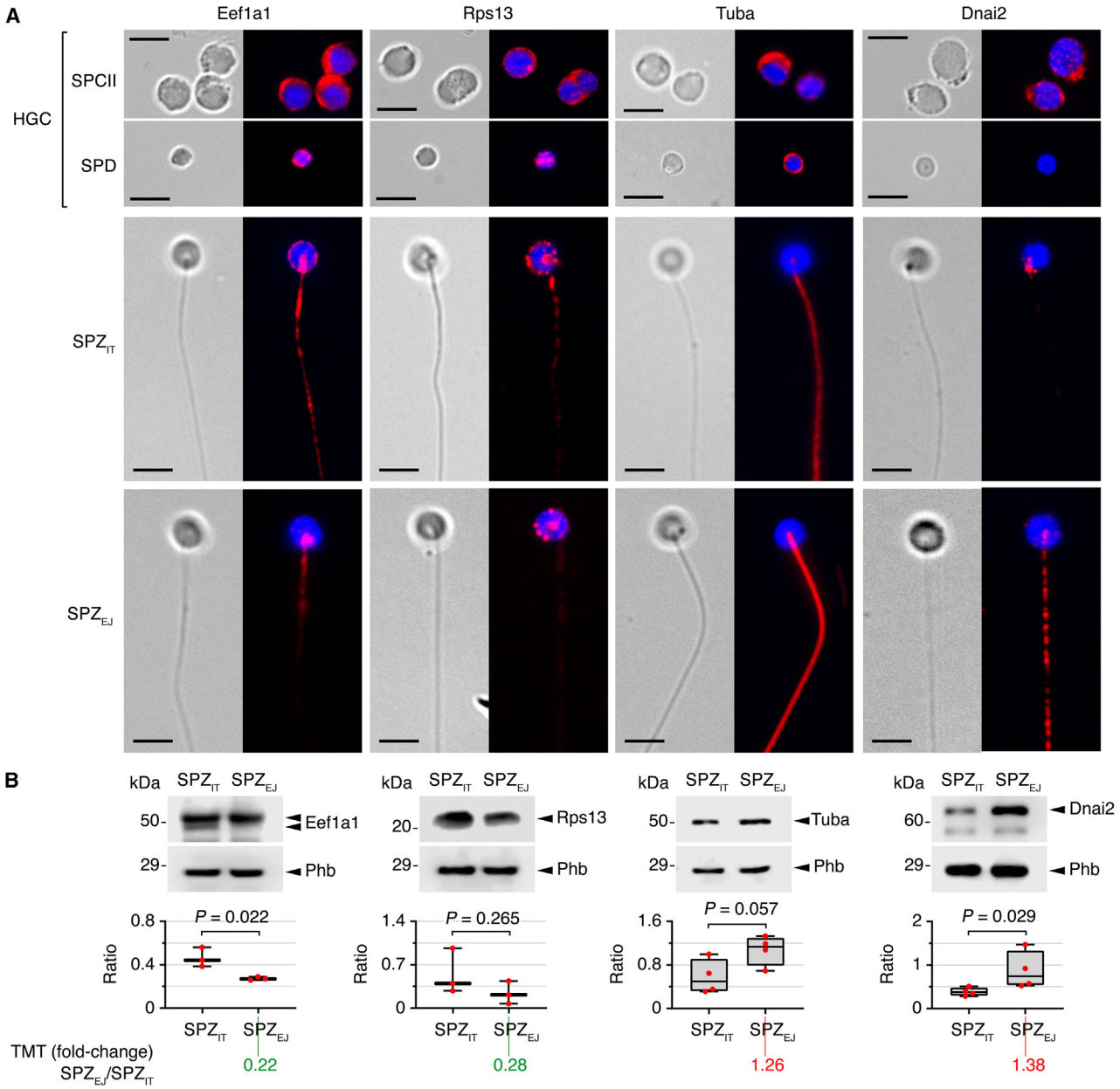

Figure 4. Immunofluorescence microscopy and immunoblot evaluation of differentially accumulated proteins in SPZ_{IT} and SPZ_{EJ}

(A) Representative immunostaining of eukaryotic translation elongation factor 1 alpha 1 (Eef1a1), 40S ribosomal protein S13 (Rps13), α-tubulin (Tuba) and dynein axonemal intermediate chain 2 (Dnai2) in haploid spermatocytes II (SPCII), spermatids (SPD), SPZ_{IT} and SPZ_{EJ}. For each cell type, representative brightfield (left panels) and epifluorescence (right panels) images are shown. The nucleus is counterstained with 4′,6-diamidino-2-phenylindole dihydrochloride (DAPI; blue). Scale bars, 2 and 5 μm.

(B) Immunoblots of Eefa1, Rps13, Tuba and Dnai2 in SPZ_{IT} and SPZ_{EJ} (upper panels) and corresponding quantitation normalized to prohibitin (Phb) (lower panels). The data points (red dots) are presented as box and whisker plots/scatter dots with horizontal line (inside box) indicating median and outliers (n = 3–4 fish different from those employed for MS analyses). Statistical differences in protein abundance between SPZ_{IT} and SPZ_{EJ} were determined by the Student's t test (p-values indicated in each panel). Molecular mass markers (kDa) are on the left. The corresponding MS quantification data are presented below the plots.

Finally, Dnai2 polypeptides were only detected in discrete areas around the head of SPZ_{IT}, while in SPZ_{EJ} the staining was distributed along the flagellum (Figure 4A).

For the immunoblotting experiments, prohibitin (Phb) was employed as an endogenous control to normalize the abundance levels of targeted proteins. These analyses showed an accumulation profile of Eef1a1, Rps13, Tuba and Dnai2 in SPZ_{IT} or SPZ_{EJ} that closely paralleled the trends identified by MS analyses. However, in these experiments statistically significant differences were only detected for Eef1a1 and Dnai2 (Figure 4B).

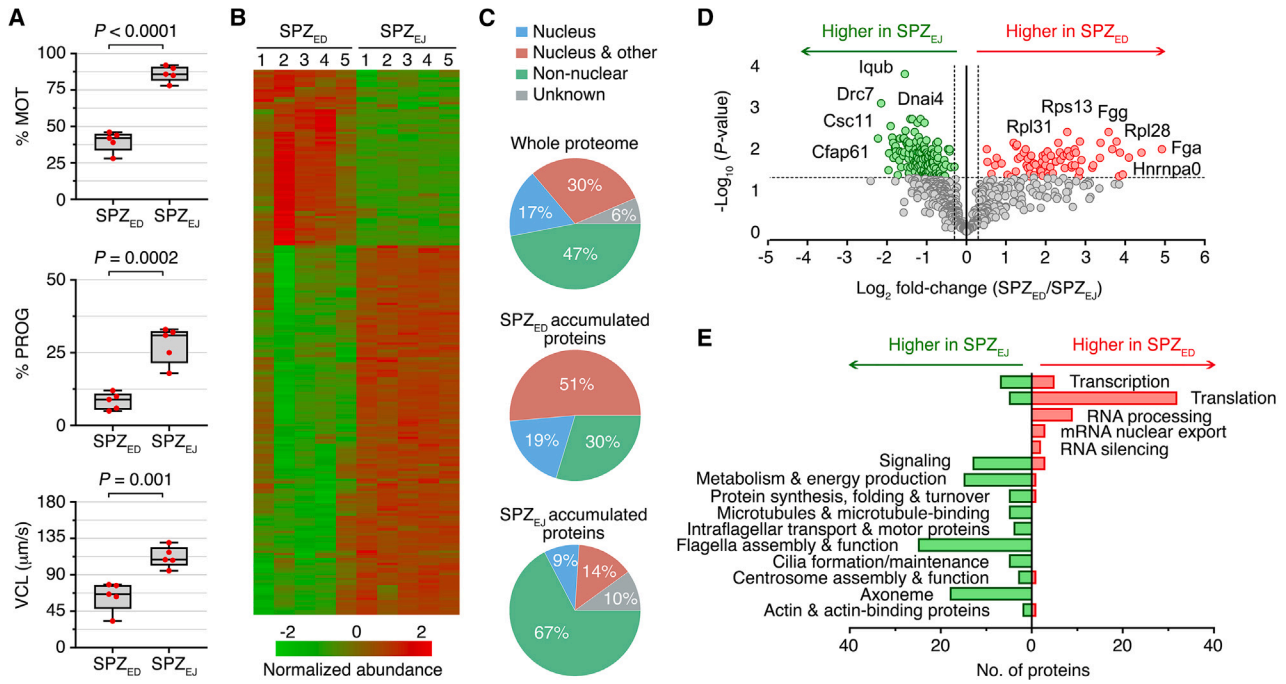

Figure 5. Changes of the nuclear-enriched proteome profile during sperm maturation

(A) Percentage of motility (% MOT), progressivity (% PROG) and curvilinear velocity (VCL) of immature spermatozoa collected from the efferent duct (SPZ_{ED}) and ejaculated spermatozoa (SPZ_{EJ}). The data points (red dots) are presented as box and whisker plots/scatter dots with horizontal line (inside box) indicating median and outliers (n = 5 males). Statistical differences were measured by the Student's t test or by the nonparametric Mann-Whitney test, and the calculated p-values are indicated in each plot.

(B) Hierarchical clustering heatmap of normalized protein abundance of 224 differentially accumulated proteins (p-value <0.05; ±1.15-fold change) between SPZ_{ED} and SPZ_{EJ}.

(C) Predicted subcellular localization of the proteins from the whole proteome identified, and of the proteins differentially accumulated in SPZ_{ED} or SPZ_{EJ}, according to GO information based on Cellular component.

(D) Volcano plot depicting the $\log_2$ fold change in expression (x axis) and the negative logarithm of their p-value to base 10 (y axis) of all the identified proteins (704) changing between SPZ_{ED} and SPZ_{EJ}. Proteins were determined to be differentially accumulated as in B. Several proteins that showed prominent fold changes are annotated.

(E) Functional annotation of differentially accumulated proteins in SPZ_{ED} and SPZ_{EJ} based on GO analysis and the Uniprot database.

Changes of the nuclear-enriched proteome profile during sperm maturation

To further investigate whether seabream spermatozoa can synthesize proteins *de novo* during the maturation phase, we carried out an additional LC-MS/MS analysis employing nuclear enriched samples from immature spermatozoa and SPZ_{EJ}. As representative of the immature stage, in this experiment we used spermatozoa directly collected from the ED (SPZ_{ED}) in order to minimize potential contamination by HCG or other somatic cells (Figure 1A). Time-course monitoring of the motion kinetics of SPZ_{ED} and SPZ_{EJ} upon seawater activation using CASA confirmed that SPZ_{ED} show a reduced %MOT, %PROG, and VCL with respect to SPZ_{EJ} (Figure 5A), thus confirming that SPZ_{ED} can be classified as immature gametes as the SPZ_{IT}.

The quantitative evaluation of protein abundance between SPZ_{ED} and SPZ_{EJ} was carried out on five biological replicates per each cell type, each replicate representing one different male. The PCA of the expression data showed that each spermatozoon population was clearly differentiated on the basis of their changing proteome (Figure S2). However, while the five SPZ_{EJ} biological replicates clustered very closely, those of SPZ_{ED} were more distant, suggesting that these spermatozoa were possibly at different stages during maturation when they were collected from the ED. Nevertheless, the MS analysis identified 704 unique proteins, from which we identified 220 significantly differentially accumulated proteins between SPZ_{ED} and SPZ_{EJ} (Figure 5B, Tables S7 and S8). Annotation of the proteins of the whole proteome according to GO information based on cellular component, revealed that half of the identified proteins with known locations (47%) were either putatively expressed in only the nucleus or in the nucleus plus other regions of the cell (Figure 5C). However, a substantial portion of the differentially accumulated proteins in SPZ_{ED} (70%) showed a putative nuclear localization, whereas most of the proteins differentially expressed in SPZ_{EJ} (67%) mapped to non-nuclear locations (Figure 5C).

The quantitative changes in SPZ_{ED} assessed via volcano plots included 74 proteins that experienced ≥2.5-fold changes with respect to SPZ_{EJ} (Figure 5D and Table S7). The most dominant among these were fibrinogen alpha chain (Fga), heterogeneous nuclear ribonucleoprotein A0 (Hnrnpa0) and fibrinogen gamma chain (Fgg). Other notably accumulated proteins in SPZ_{ED}

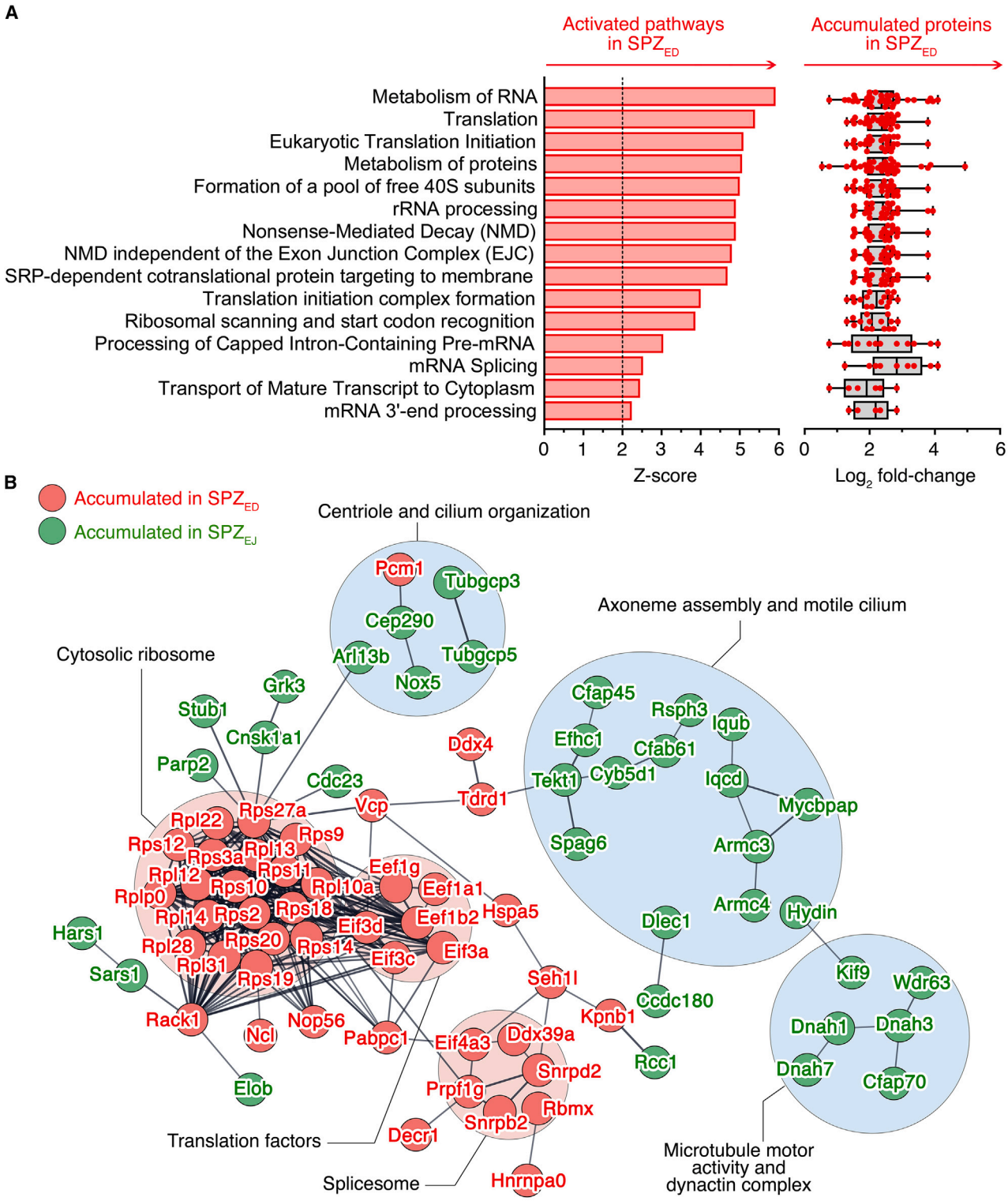

Figure 6. Pathways analysis and protein-protein interaction networks during spermatozoon maturation

(A) Canonical pathways related to protein abundance changes in SPZ_{ED} identified using PANTHER and Reactome database (left panel), and log_2 fold change of the proteins within each pathway (right panel). A *Z* score of ±2 was considered predictive of activation/inhibition of the identified pathway. Only activated pathways are shown because the inhibition pathways did not pass the *Z* score.

(legend continued on next page)

included ribosomal protein L28 (Rpl28), Rps13 and 60S ribosomal protein L31 (Rpl31). Conversely, 150 proteins were more accumulated in SPZ_{EJ} (1.5– to2.2-fold increase) than in SPZ_{ED}, with most of them having been previously implicated in the regulation of sperm motility, such as cilia and flagella associated protein 61 (Cfap61), dynein regulatory complex subunit 7 (Drc7), dynein axonemal intermediate chain 4 (Dnai4), IQ and ubiquitin-like domain-containing protein (Iqub) and calcium permeable stress-gated cation channel 1-like protein 1 (Csc11) (Figure 5D and Table S7). Further functional annotation of differentially accumulated proteins into SPZ_{ED} or SPZ_{EJ}, indicated a higher abundance of proteins related to transcription, RNA processing and translation in SPZ_{ED} (5, 9 and 32 proteins, respectively) (Figure 5E). In contrast, the majority of proteins accumulated in SPZ_{EJ} were related to the formation of the cytoskeleton and cell movement, such as flagella assembly and function and axoneme, although other notable enriched functional categories in SPZ_{EJ} were metabolism and energy dissipation and signaling (25, 18, 15 and 13 proteins, respectively) (Figure 5E).

Seeking to understand the biological processes associated with changes in protein composition during sperm maturation, we finally performed pathway analysis of the differentially accumulated proteins using Panther and the Reactome database.[38] This analysis identified 15 enriched pathways predicted to be activated in $SPZ_{ED,}$ while none was predicted to be activated in SPZ_{EJ} (*Z* score not significant) (Figure 6A). In SPZ_{ED}, the top five activated pathways (*Z* score 5 to 6) were metabolism of RNA (ID R-MMU-8953854), translation (ID R-MMU-72766), eukaryotic translation initiation (ID R-MMU-72613), metabolism of proteins (ID R-MMU-392499) and formation of a pool of free 40S subunits (ID R-MMU-72689). Moreover, other activated predicted pathways in SPZ_{ED} (*Z* score 2.5 to 4) were ribosomal scanning and start codon recognition (ID R-MMU-72702), processing of capped intron-containing pre-mRNA (ID R-MMU-72203), and mRNA splicing (ID R-MMU-72172). To further complement this analysis, we built a PPI network combining the proteins differentially accumulated in either SPZ_{ED} or SPZ_{EJ} using STRING. A connected network of 172 proteins and 310 connections was mapped, where the proteins could be grouped into six subclusters (Figure 6B). Most of the proteins accumulated in SPZ_{ED} were grouped into the cytosolic ribosome, translation factors and spliceosome subclusters. In contrast, the differentially abundant proteins in SPZ_{EJ} were predominantly included in subclusters related to flagellum organization, microtubule motor activity and dynactin complex. These data corroborate our previous observations, suggesting that seabream spermatozoa may be translationally competent during their maturation in the ETDs.

Seabream spermatozoa can conduct *de novo* protein synthesis

To investigate whether protein translation can occur in immature spermatozoa, we first corroborated that ribosomal and flagellar proteins were more accumulated in SPZ_{ED} and SPZ_{EJ}, respectively. For this, we analyzed the presence of selected cytosolic ribosomal proteins, such as Rpl31, small ribosomal subunit protein uS5 (Rps2) and Rps13, and proteins from the flagellar axoneme, Spag6, Dynll2 and Tuba, in SPZ_{ED} and SPZ_{EJ} by immunofluorescence microscopy and immunoblotting using commercial antibodies as above. In addition, although not detected as differentially accumulated proteins in the MS analysis, we also examined the abundance of two mitochondrial ribosomes, the small ribosomal subunit protein uS5m (mRps5) and the large ribosomal subunit protein bL28m (mRpl28), the mRNAs of which has previously been detected in seabream SPZ_{EJ}.[31] In SPZ_{ED}, the staining obtained for the three ribosomal proteins investigated was similar, being localized in the head as perinuclear and intranuclear, while the signals remained in the same regions in SPZ_{EJ} but with somewhat less intensity (Figures 7A–7C, upper panels). Semiquantitative immunoblotting, using Phb or histone 3 (H3) as endogenous controls, in individual fish (n = 3–4) different from those employed for MS analyses, indicated a higher accumulation of Rpl31, Rps2 and Rps13 in SPZ_{ED} as observed by MS, although the differences were only statistically significant for Rps13 (Figures 7A–7C, lower panels). The axoneme proteins Spag6, Dynll2 and Tuba were specifically localized along the flagellum, and each of them were significantly more accumulated in SPZ_{EJ} in agreement with the MS data (Figures 7D–7F). Finally, both mitochondrial ribosomes co-localized with the spermatozoon mitochondrion, as revealed when sperm cells were previously loaded with the mitochondrion-specific vital dye MitoTracker Green FM, and no differences were detected between SPZ_{ED} and SPZ_{EJ} by either immunostaining (Figures 7G and 7H) or immunoblotting (Figure S3).

Since ribosomal proteins were detected in both SPZ_{ED} and SPZ_{EJ}, we next aimed to obtain experimental evidence of translational activity in spermatozoa. For this, isolated SPZ_{ED} and SPZ_{EJ} were incubated *in vitro* in the presence of charged lysine transfer RNA (tRNA) tagged with BODIPY-FL ($tRNA^{Lys}$-BODIPY-FL) that labels newly made polypeptides in permeabilized spermatozoa. In these experiments, freshly collected sperm was diluted 300 times in non-activating medium (NAM) to avoid contamination by remnants of somatic cells or HGC, which was also confirmed by fluorescence microscopy and flow cytometry of the diluted samples (Figure S4). At different times during the incubation period, aliquots of spermatozoa were collected, extracted, and immunoblotted using an anti-BODIPY-FL antibody. The results showed that SPZ_{ED} were able to incorporate $tRNA^{Lys}$-BODIPY-FL in vitro as indicated by the progressive increase in the intensity of different polypeptide bands of ~55, ~45, ~31 and ~28 kDa in the total cell lysates up to 20 h of incubation (Figure 8A). The BODIPY-FL reactive bands were not revealed in extracts from SPZ_{ED} incubated for 20 h in the absence of $tRNA^{Lys}$-BODIPY-FL, indicating the specificity of the signals (Figure 8A). A similar trend in $tRNA^{Lys}$-BODIPY-FL incorporation was observed in SPZ_{EJ}, although the reactive polypeptide bands detected in their extracts were less intense

(B) The protein-protein interaction networks of differentially accumulated proteins in SPZ_{ED} or SPZ_{EJ} obtained using STRING database v11.5 with a high confidence interaction score (0.7). Proteins and their interactions are shown as nodes (spheres) and edges (lines), respectively. Nodes in red or green color indicate protein accumulation in SPZ_{ED} or SPZ_{EJ}, respectively. Proteins are grouped based on STRING network clusters and KEGG pathways.

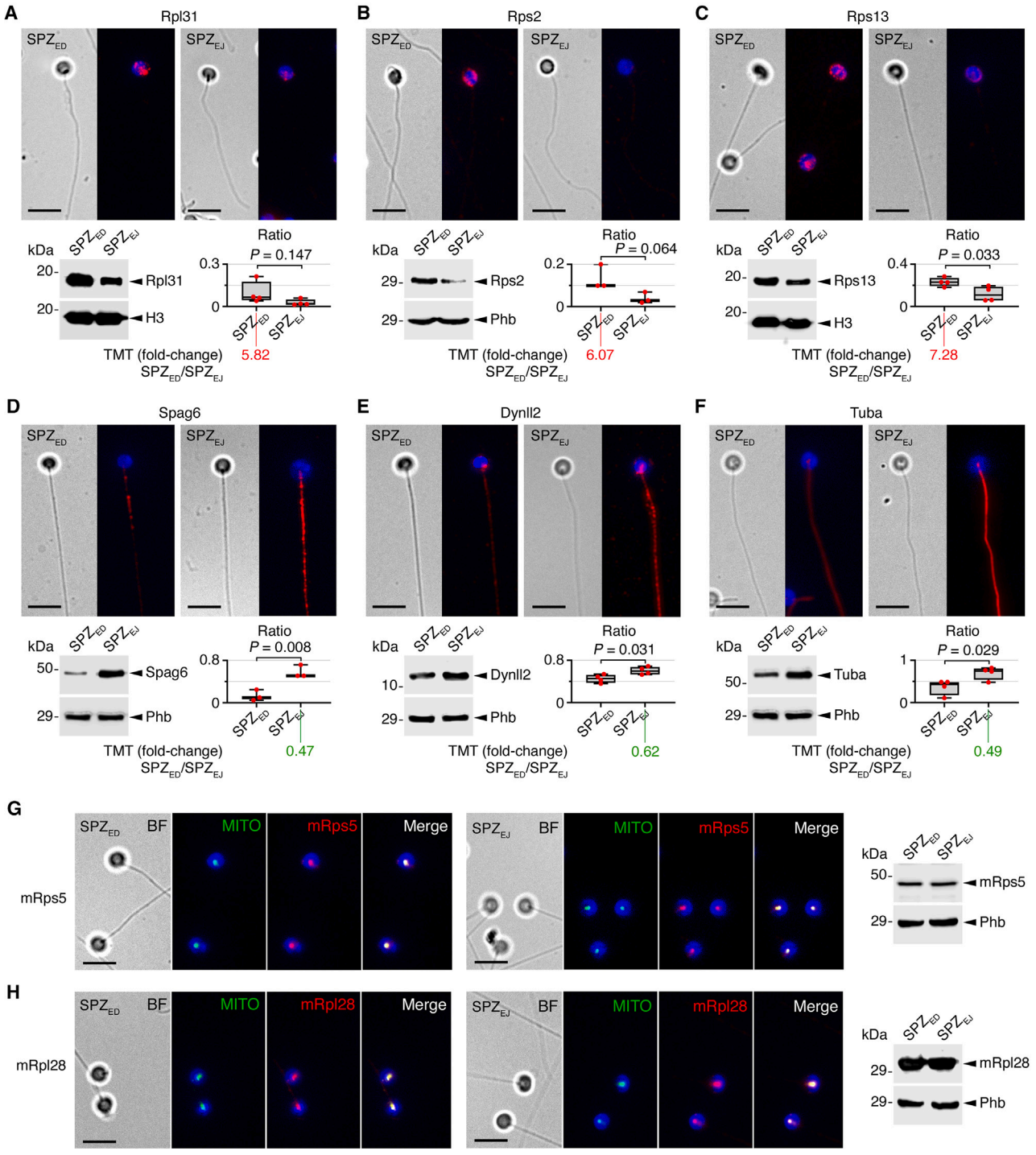

Figure 7. Immunostaining and immunoblot of ribosomal and motility-related proteins in SPZ_{ED} and SPZ_{EJ}

(A–F) The upper panels show representative immunostaining of large ribosomal subunit protein eL31 (Rpl31, A), small ribosomal subunit protein uS5 (Rps2, B), 40S ribosomal protein S13 (Rps13, C), sperm-associated antigen 6 (Spag6, D), dynein light chain 2 (Dynll2, E) and α-tubulin (Tuba, F) in SPZ_{ED} and SPZ_{EJ}. The brightfield (left) and epifluorescence (right) images with the nucleus counterstained with DAPI (blue) are shown. Scale bars, 5 μm. The lower panels depict the corresponding immunoblots (left) and quantitation normalized to prohibitin (Phb) or histone H3 (H3) (right). The data points (red dots) are presented as box and whisker plots/scatter dots with horizontal line (inside box) indicating median and outliers (n = 3–4 fish different from those employed for MS analyses). Statistical differences in protein abundance between SPZ_{ED} and SPZ_{EJ} were determined by an unpaired Student's t test (p-values indicated above each plot). Molecular mass markers (kDa) are on the left, and the corresponding MS quantification data are presented below the plots.

(legend continued on next page)

than those from the SPZ_{ED}, and some cross-reactive bands were detected in sperm not exposed to Lys-charged tRNA for 20 h (Figure 8A). To visualize the cellular sites of the nascent translated proteins within SPZ_{ED}, we used immunofluorescence microscopy, which showed high BODIPY-FL staining intensity in the head around the nucleus, including the mitochondrion, and relatively low signal in the most anterior part of the tail (Figure 8B). Therefore, the spatial accumulation of *de novo* translated proteins in the spermatozoon cytoplasm largely coincided with that of the Rps2, Rps13, Rpl31, mRps5 and mRpl28 proteins from the small and large subunits of cytoplasmic and mitochondrial ribosomes. These findings suggested that seabream SPZ_{ED} and SPZ_{EJ} may be translationally competent.

To investigate the underlying translational mechanisms in spermatozoa, we carried out further experiments *in vitro* in which SPZ_{ED}, which apparently showed stronger translation activity than SPZ_{EJ}, were incubated with $tRNA^{Lys}$-BODIPY-FL in the presence of the mitochondrial translation inhibitor D-chloramphenicol (CP), the cytoplasmic translation inhibitor cycloheximide (CHX), or the drugs vehicle. To determine whether the possible sources of the corresponding mRNAs in sperm could be newly transcribed mRNA molecules in addition to long-lasting mRNA, we also applied the transcription inhibitor actinomycin D (ActD). In the extracts from sperm treated with CHX, CP or AcD the intensity of the BODIPY-FL reactive bands of ~55, ~45 and ~31 kDa, as well as of a band of ~200 kDa which could not be detected in the previous experiments, was lower than those in the vehicle-exposed spermatozoa (control) (Figure 8C). These observations suggest that protein translation in seabream sperm involves both mitochondrial and cytoplasmic ribosomes. In addition, the data indicate that *de novo* transcription could also take place in maturing spermatozoa.

The physiological importance of protein synthesis in sperm was evaluated by testing the motility of SPZ_{EJ} incubated with CHX and CP for 13 h prior to seawater activation. Sperm vitality staining at the end of the incubation showed that the mitochondrial membrane potential of sperm cells was not altered after long-term treatment with the inhibitors, indicating that the capacity of mitochondria to produce ATP to support sperm motility remained intact (Figure 8D). However, treatment with CHX reduced the % MOT and % PROG by 33% and 41%, respectively, whereas CP blocked these kinetic parameters by 40% and 52%, respectively (Figures 8E and 8F). These data therefore indicate that active translation of motility-related proteins in seabream spermatozoa is needed for full sperm function.

Seabream SPZ_{ED} can translate nuclear-encoded proteins by cytoplasmic- and mitochondrial-type ribosomes

Total RNA in seabream spermatozoa has a size distribution showing the 18S and 28S rRNA peaks[31] (Figure S5). To obtain further support for cytoplasmic and mitochondrial translation in seabream sperm, we analyzed the activation state of ribosomes and some motility-related proteins in SPZ_{ED} by means of sucrose gradient fractionation of spermatozoa, followed by RT-PCR and immunoblotting. The components of the large and small subunits of the cytoplasmic 80S (28S and 18S rRNAs, respectively) and mitochondrial 55S (16S and 12S rRNAs, respectively) ribosomes, as well as the Rpl31, Rps2, mRpl28 and mRps5, were found with low-density fractions, corresponding to ribonucleoproteins and single ribosomal particles (monosomes), as well as with the high-density fractions containing multi-ribosomal particles (polysomes) (Figures 9D and 9E). The presence of 80S and 55S ribosomes and associated proteins in the polysomal fractions shows that both ribonucleoprotein complexes are actively involved in sperm protein translation. The Dynll2 mRNA and protein, together with *drc7* and *cfap61* mRNAs and Spag6, were also present in the low-density and polysomal fractions of SPZ_{ED} (Figures 9D and 9E). These data agree with the higher abundance of these flagellar-associated proteins in SPZ_{EJ} with respect to SPZ_{ED} previously observed, suggesting that proteins involved in sperm motility are likely to be translated in spermatozoa.

To validate these analyses, we determined the presence of the heat shock protein 90 (Hsp90) as negative control, since its abundance in SPZ_{ED} did not significantly change with respect to that in SPZ_{EJ} in the MS analyses (fold change of 0.65; $p = 0.099$). As a further control, we used aquaporin-3a (Aqp3a), which is detected in seabream spermatozoa, but not in testicular somatic cells or HGC.[39] In addition, Aqp3a translation increases during seabream sperm maturation and is essential for osmoadaptation of the post-activated spermatozoon.[39] The Hsp90 mRNA and protein were exclusively found with the initial low density fractions (fractions 1 to 6) (Figures 9D and 9E), according to the apparent absence of translation of this protein in SPZ_{ED}, whereas the Aqp3a polypeptides were detected in all fractions, including the monosomal and polysomal fractions (Figure 9E). These data therefore reinforce the notion that both cytoplasmic and mitochondrial translation occurs in seabream spermatozoa, thereby enhancing the synthesis of proteins involved in flagellar motility and sperm osmoadaptation.

DISCUSSION

In contrast to mammals, post-testicular maturation mechanisms of piscine spermatozoa are completely unknown. Here, we have employed quantitative proteomics to report the changes in the teleost sperm proteome between the intratesticular differentiation and the extratesticular maturation stages. Our data show that a substantial remodeling of protein expression occurs during these developmental processes, which appears to be necessary for the acquisition of full spermatozoon function. Moreover, we provide evidence that both 80S cytosolic and 55S mitochondrial ribosomes conduct *de novo* protein translation during post-testicular sperm development.

(G and H) Representative immunostaining of small mitochondrial ribosomal subunit uS5m (mRps5, A) and large mitochondrial ribosomal subunit bL28m (mRpl28, B) in SPZ_{ED} and SPZ_{EJ}. The nucleus was counterstained with 4′,6-diamidino-2-phenylindole dihydrochloride (DAPI; blue), whereas the spermatozoon mitochondrion was labeled with MitoTracker Green FM (green). Scale bars, 5 μm. To the right of each panel the corresponding immunoblots using PhB as loading control are shown. Molecular mass markers (kDa) are on the left.

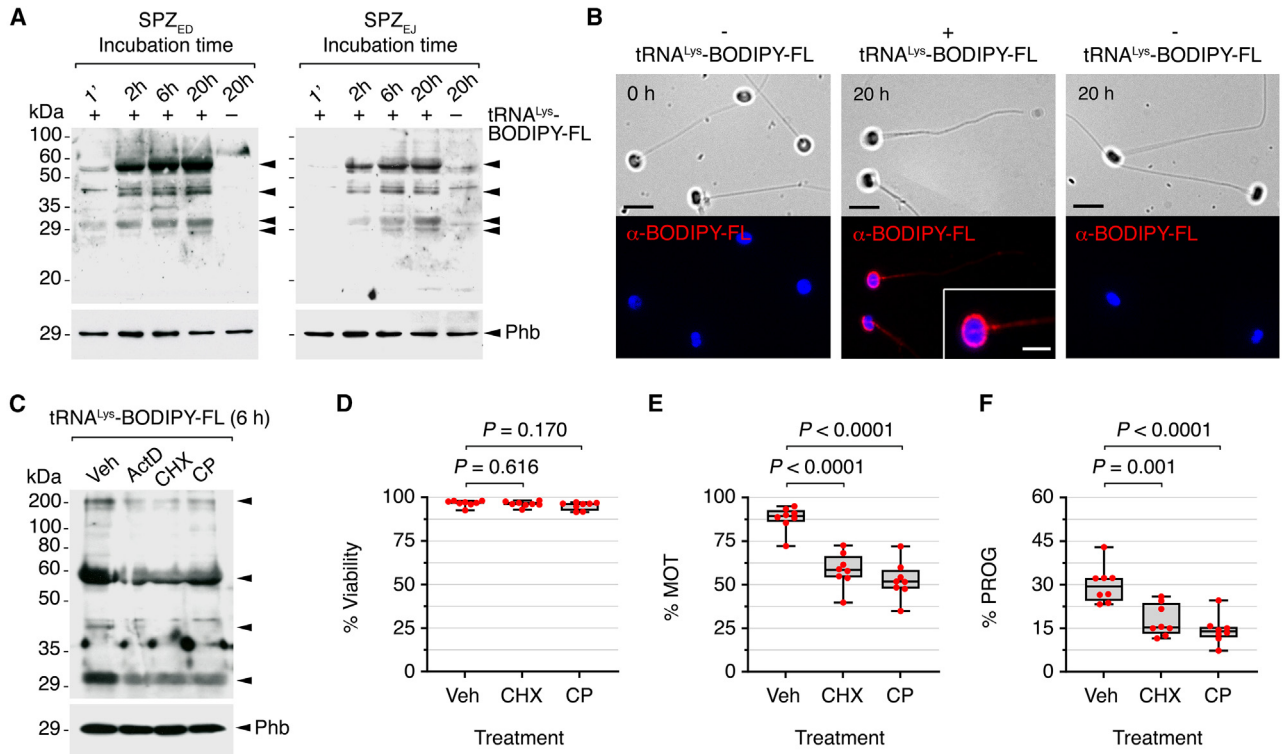

Figure 8. Seabream spermatozoa can conduct *de novo* protein synthesis

(A) SDS-PAGE and immunoblot analysis of *in vitro* translated products by isolated SPZ_{ED} (left) and SPZ_{EJ} (right) incubated *in vitro* with charged lysine-tRNAs labeled with the fluorophore BODIPY-FL ($tRNA^{Lys}$-BODIPY-FL) for 1 min, or 2, 6 and 20 h. *De novo* translated polypeptides (arrowheads) were detected with an anti-BODIPY-FL antibody. The negative controls were incubated without BODIPY-FL for 20 h. The arrowheads indicate the progressive increase in the intensity of different reactive polypeptide bands. Prohibitin (Phb) was used to verify equal loading (lower blot). Molecular mass markers (kDa) are to the left.

(B) Immunolocalization of *de novo* translated proteins in SPZ_{ED} treated as in A for 20 h using the anti-BODIPY-FL antibody. Scale bars, 5 μm.

(C) Immunoblot of *de novo* translated products by isolated SPZ_{ED} incubated with $tRNA^{Lys}$-BODIPY-FL for 6 h in the presence of 100 μg/mL of transcription (actinomycin D, ActD) or translation (cycloheximide and chloramphenicol; CHX and CP, respectively) inhibitors, or the drug vehicles (0.5% DMSO or 0.5% ethanol). The arrowheads indicate BODIPY-labelled polypeptides, the intensity of which is reduced in the presence of the inhibitors. As above, Phb was used to verify equal loading (lower blot). Molecular mass markers (kDa) are to the left.

(D–F) Percentage of viable spermatozoa (D), % MOT (E) and % PROG (F) of SPZ_{EJ} previously incubated with Veh (0.5% ethanol), CHX or CP for 13 h as above before activation. The data points (red dots) are presented as box and whisker plots/scatter dots with horizontal line (inside box) indicating median and outliers (n = 8 males). Statistical differences were measured by one-way ANOVA followed by the Dunnett's multiple comparisons test, and the calculated p-values are indicated in brackets in each plot.

The present global proteome analyses of seabream sperm suggest a model in which proteins potentially involved in translation, mRNA processing and protein synthesis, folding and turnover are predominantly accumulated in maturing spermatozoa (SPZ_{IT} and SPZ_{ED}), while proteins related to flagellar motility and metabolism and energy production are in general more enriched in mature sperm (SPZ_{EJ}). In immature spermatozoa, we found a higher accumulation of many structural components of cytosolic ribosomes, different translation initiation and elongation factors, and components of the spliceosome. Immature sperm cells also accumulate components of the PIWI/PIWI-interacting RNA (PIWI/piRNA) pathway involved in the translational activation of spermiogenic mRNAs,[40] as well as components of the 26S proteasome proteolytic machinery that typically maintain the motility and fertilization potential of the spermatozoon.[41–43] In addition, we found higher accumulation of members of the chaperonin containing T-complex/TCP1-ring complex (CCT/TRiC) involved in chaperone-assisted correct protein folding of cytoskeletal and cytosolic proteins.[44] Overall, these data indicate that mechanisms of protein turnover and folding are potentially involved during seabream spermatozoon differentiation and maturation, as described in mammals,[45] and they would also be consistent with the presence of translational activities in the immature spermatozoa.

By contrast, seabream mature sperm were enriched in protein components of the axoneme, which are likely necessary for flagellar assembly and function, such as several dyneins (Dynll2, Dnali1, Dnah2, Dnah7, Dnah8, and Dnah12), cilia- and flagella-associated proteins (Cfap20, -45L, -53, -206), dynein regulatory complex (Ccdc65, Drc1 and -7), and sperm flagellar proteins (Spef2).[46] Other important proteins required for axoneme assembly or flagellar beating also accumulated in mature sperm including Tekt1,[47] Ropn1,[48] Spag6,[49] and Kif9.[50] In these cells, we also detected more proteins putatively related to metabolism

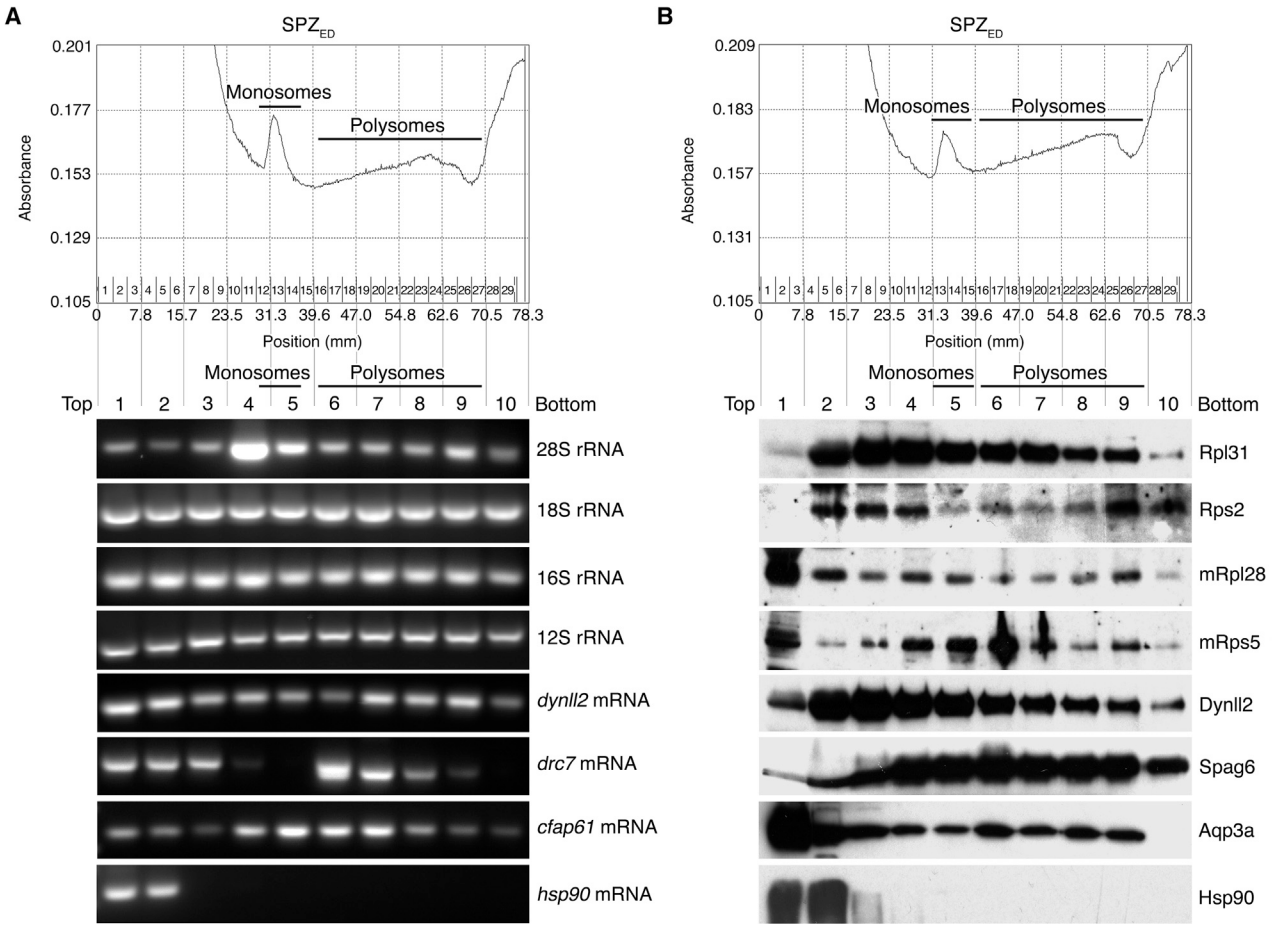

Figure 9. Seabream SPZ_{ED} can translate nuclear-encoded proteins by cytoplasmic- and mitochondrial-type ribosomes

(A and B) Representative sucrose gradient fractionations of SPZ_{ED} extracts, where the absorbance at 260 nm was measured in each of the 30 fractions collected, showing the distribution of single (monosomes) and multi ribosomal particles (polysomes). In A, below the panel is shown the RT-PCR detection in the fractions from the gradient (pooled into 10 samples as indicated) of ribosomal RNAs of the 80S cytoplasmic (28S and 18S rRNAs) and 55S mitochondrial (16S and 12S rRNAs) ribosomes, and of mRNAs encoding for differentially accumulated proteins in SPZ_{ED} identified in the MS analysis (*dynll2*, *drc7,* and *cfap61*). The *hsp90* mRNA was used as a negative control. In (B), the lower panel shows the analysis by western blot of cytoplasmic (Rpl31 and Rps2) and mitochondrial (mRpl28 and mRps5) ribosomal proteins, motility-related proteins (Dynll2 and Spag6), and control proteins (Aqp3a and Hsp90), in each of the 10 pooled samples.

and energy dissipation than in immature spermatozoa, although in most cases the abundance of these proteins was not statistically different. Nevertheless, our analysis confirmed the presence of different enzymes potentially involved in the TCA cycle and OXPHOS, which seem to be the major metabolic pathways that sustain motility of seabream spermatozoa.[51–53] Finally, we identified proteins related to the removal of superoxide radicals and peroxidase activity highly accumulated in mature sperm, which are possibly essential to prevent oxidative stress in sperm caused by both OXPHOS and osmotic stress upon ejaculation into the hyperosmotic sea.[53,54]

Consistent with the MS analyses, we were able to immunolocalize both cytosolic and mitochondrial ribosomal proteins in immature as well as mature seabream spermatozoa. In mammalian spermatozoa, the presence of cytosolic ribosomes has also been demonstrated,[17,55] although its functional significance is questioned since during spermiogenesis most of the sperm cytoplasm is eliminated in the form of "residual bodies" that are phagocytosed by Sertoli cells.[56] Therefore, most studies suggest that only mitochondrial translation occurs during sperm capacitation.[12,14–17] In our study, the MS analyses indicated that cytosolic ribosomal proteins were more accumulated in immature than in mature spermatozoa, although statistical analysis of semiquantitative immunoblot densitometry only confirmed this observation for Rps13. Nevertheless, the presence of ribosomal proteins in seabream immature sperm, and the subsequent increase of proteins potentially involved in flagellar function and ATP synthesis in mature spermatozoa, prompted us to speculate that the translation of motility-related factors may be upregulated during the maturation of the spermatozoon. In support of this hypothesis, we found that immature spermatozoa are capable of *de novo* protein synthesis *in vitro*, which could be reduced by CHX as well as by CP, thus suggesting, in contrast to mammals, the presence of both cytoplasmic and mitochondrial translation in the seabream spermatozoa. Motility assays and $tRNA^{Lys}$-BODIPY-FL incorporation data further indicated that

such translational activities are retained in ejaculated (mature) spermatozoa, which could contribute to flagellar motility maintenance upon activation. It is therefore likely that seabream spermatozoa synthesize new proteins needed for motility during the maturation phase in the ETDs, as well as replace proteins that have degraded before and after ejaculation.

Sucrose gradient fractionation experiments showed that the polysomal fractions of immature sperm were based on cytosolic and mitochondrial ribosomes, thus further supporting our conclusion that cytoplasmic as well as mitochondrial translation takes place in post-testicular seabream spermatozoa. The detection of mRNA and/or protein for Dynll2, Drc7, Cfap61 and Aqp3a in the polysomal fraction provides additional evidence that proteins associated with flagellar beating and sperm osmoadaptation are actively translated in spermatozoa during the maturation phase. The presence of mitochondrial ribosomes outside the mitochondria has been suggested as a possible mechanism in sperm to explain the potential synthesis of nuclear-encoded proteins by mitochondrial ribosomes.[12,57] Here, we found that the mRps5 and mRpl28 are apparently localized inside the spermatozoon mitochondrion, but since seabream spermatozoa express about 60 different mRNAs encoding for mitochondrial ribosomal proteins,[31] it is still possible that a similar mechanism to that suggested for mammals may exist in seabream sperm. In any event, our findings may suggest that *de novo* translation of nuclear-encoded proteins in teleost spermatozoa and mammalian sperm undergoing capacitation may be a widespread mechanism across vertebrate species for the acquisition of full motility potential.

An intriguing observation in our study was that the transcription inhibitor ActD was able to partially prevent protein synthesis in immature spermatozoa and impaired the motility of ejaculated sperm upon activation, suggesting that translation may be in part transcription-dependent. In ejaculated boar spermatozoa, both mitochondrial transcription and translation are active,[16] which could be potentially inhibited by ActD.[58] Therefore, it is plausible that the negative effect of ActD on protein synthesis that we observed in seabream sperm is related to mitochondrial transcription, since it is believed that nuclear transcription in sperm remains virtually silent.[59–61] However, it has been shown that the expression of transcripts in zebrafish (*Danio rerio*) mature sperm correlates with specific histone modifications in the chromatin associated with active transcription (H3K4me2/3 or H3K14ac), as well as with DNA hypomethylation.[61] Such regions of active chromatin have been related with the activation of genes involved in microtubule organization, protein metabolism or intracellular transport in early embryos before the activation of the zygotic genome.[61] Nevertheless, it is not known when H3K4me2/3 and H3K14ac, or other active chromatin marks, are accumulated in the fish sperm chromatin during spermiogenesis, and whether this mechanism can activate gene transcription during the maturation of spermatozoa. In support of this hypothesis, we observed that immature spermatozoa accumulate putative transcriptional regulators, such as Myb-binding protein 1a and nucleolin,[62,63] as well as the H3K79-specific histone-Lys N-methyltransferase, which dimethylates H3K79m2,[64] leading to transcription activation in somatic cells.[65] We also noted a higher accumulation in mature sperm of additional potential transcriptional regulators, such as chromodomain-helicase-DNA-binding protein 1, transcription termination factor 1, elongin-B and MLX-interacting protein. These proteins could however represent remnant products from the maturation phase or correspond to proteins required to activate gene transcription following fertilization. Our observations are thus not conclusive, and therefore, whether seabream and zebrafish spermatozoa, both of which lack protamines in the chromatin,[61,66] are transcriptionally active remains to be clarified.

In summary, the present study analyzed proteomic changes induced during the differentiation and maturation of spermatozoa of the teleost gilthead seabream, providing preliminary insights into the molecular pathways involved in the formation of fertilization competent spermatozoa in fish. The data also revealed that seabream spermatozoa utilize cytosolic and mitochondrial ribosomes and are translationally active during their maturation phase within the ETDs, which appears to be sustained post-ejaculation. Such late-stage translational mechanisms might be essential to replace degraded proteins while spermatozoa transit and exit the ETDs, as well as to activate the translation of specific mRNAs essential for the acquisition of full sperm function and fertility competence.

Limitations of the study

The current study reports a systematic and comprehensive proteomic landscape during fish spermiogenesis and sperm maturation. However, the number of proteins identified were limited and thus they represent a snapshot of the changes in the proteome that occurs during these developmental processes. Further studies will therefore be necessary to establish the complete proteomic signatures of sperm differentiation and maturation in fish. In addition, although we provide evidence indicating that maturing seabream spermatozoa are translationally active, the total number and identity of the proteins that are translated specifically at this stage remain to be uncovered. Further approaches to uncover potential *de novo* transcriptional mechanisms in spermatozoa could also provide deeper insights into the transcriptional regulation during fish sperm maturation. Finally, our study was focused on a single piscine model species, and therefore whether active cytoplasmic and mitochondrial translation activities in spermatozoa is a conserved feature in teleosts is yet unknown and should be investigated in the future.

RESOURCE AVAILABILITY

Lead contact

Further information and requests for resources and reagents should be directed to and will be fulfilled by the lead contact, Joan Cerdà (jcerda@icm.csic.es).

Materials availability

This study did not generate new unique reagents.

Data and code availability

- The mass spectrometry proteomic data have been deposited at the ProteomeXchange Consortium via the PRIDE[67] partner repository, and are publicly available as of the date of publication. The accession number is listed in the key resources table.
- This paper does not report original code.

- Any additional information required to reanalyze the data reported in this paper is available from the lead contact upon request.

ACKNOWLEDGMENTS

We are very grateful to Prof. Mihaela Zavolan (Biozentrum, University of Basel, Switzerland) for providing the instrumentation required for the polysome profiles. This work was supported by the Spanish Ministry of Science, Innovation and Universities (MICIU/AEI/10.13039/501100011033) and the European Regional Development Fund (ERDF) (European Union), Grants no. AGL2016-76802-R and PID2022-138066OB-I00 (to J.C.), and by the Agency for Management of University and Research Grants (Government of Catalonia) Grant 2021 SGR 00068 (to J.C.). J.C.-A. was recipient of a predoctoral contract from Spanish MICIU (BES-2017-080778), and RNF. was supported by the University of Bergen (Norway). The authors also acknowledge the 'Severo Ochoa Centre of Excellence' accreditation (CEX2019-000928-S) funded by the Spanish Agencia Estatal de Investigación (AEI) 10.13039/501100011033.

AUTHOR CONTRIBUTIONS

J.C. designed the study. J.C.-A., F.C., A.G., and M.C. conducted the experiments. J.C.-A., F.C., A.G., M.C., and J.C. developed the methodology and analyzed the data. R.N.F. helped with data collection and analysis. J.C.-A., J.C., R.N.F., and M.C. wrote the manuscript. All authors read and approved the final paper.

DECLARATION OF INTERESTS

The authors declare no competing interests.

STAR★METHODS

Detailed methods are provided in the online version of this paper and include the following:

- KEY RESOURCES TABLE
- EXPERIMENTAL MODEL AND STUDY PARTICIPANT DETAILS
- METHOD DETAILS
  - Sperm motility assays
  - Sample preparation for LC-MS/MS quantitative proteomics
  - Protein digestion, isobaric labeling and fractionation
  - LC-MS/MS analysis
  - Immunofluorescence microscopy and immunoblotting
  - Protein labelling by $tRNA^{Lys}$ tagged with BODIPY®-FL
  - Sucrose density gradient fractionation of spermatozoa
- QUANTIFICATION AND STATISTICAL ANALYSES
  - Protein identification and quantitation by proteomic analysis
  - Protein functional classification and pathway analyses
  - Statistical analyses of sperm kinetic parameters and semiquantitative western blot

SUPPLEMENTAL INFORMATION

Supplemental information can be found online at https://doi.org/10.1016/j.isci.2024.111537.

Received: September 30, 2024
Revised: November 5, 2024
Accepted: December 3, 2024
Published: December 6, 2024

REFERENCES

1. Schulz, R.W., de França, L.R., Lareyre, J.J., Le Gac, F., Chiarini-Garcia, H., Nobrega, R.H., and Miura, T. (2010). Spermatogenesis in fish. Gen. Comp. Endocrinol. *165*, 390–411. https://doi.org/10.1016/j.ygcen.2009.02.013.
2. Nishimura, H., and L'Hernault, S.W. (2017). Spermatogenesis. Curr. Biol. *27*, R988–R994. https://doi.org/10.1016/j.cub.2017.07.067.
3. Cornwall, G.A. (2009). New insights into epididymal biology and function. Hum. Reprod. Update *15*, 213–227. https://doi.org/10.1093/humupd/dmn055.ç.
4. Pérez, L.M. (2020). Fish sperm maturation, capacitation, and motility activation. In Reproduction in Aquatic Animals, M. Yoshida and J.F. Asturiano, eds. (Springer Singapore), pp. 47–67. https://doi.org/10.1007/978-981-15-2290-1_5.
5. Sullivan, R., and Mieusset, R. (2016). The human epididymis: its function in sperm maturation. Hum. Reprod. Update *22*, 574–587. https://doi.org/10.1093/humupd/dmw015.
6. Zhang, H., Situ, C., and Guo, X. (2022). Recent progress of proteomic analysis on spermatogenesis. Biol. Reprod. *107*, 109–117. https://doi.org/10.1093/biolre/ioac065.
7. Skerget, S., Rosenow, M.A., Petritis, K., and Karr, T.L. (2015). Sperm proteome maturation in the mouse epididymis. PLoS One *10*, e0140650. https://doi.org/10.1371/journal.pone.0140650.
8. Nixon, B., De Iuliis, G.N., Hart, H.M., Zhou, W., Mathe, A., Bernstein, I.R., Anderson, A.L., Stanger, S.J., Skerrett-Byrne, D.A., Jamaluddin, M.F.B., et al. (2019). Proteomic profiling of mouse epididymosomes reveals their contributions to post-testicular sperm maturation. Mol. Cell. Proteomics *18*, S91–S108. https://doi.org/10.1074/mcp.ra118.000946.
9. Skerrett-Byrne, D.A., Anderson, A.L., Bromfield, E.G., Bernstein, I.R., Mulhall, J.E., Schjenken, J.E., Dun, M.D., Humphrey, S.J., and Nixon, B. (2022). Global profiling of the proteomic changes associated with the post-testicular maturation of mouse spermatozoa. Cell Rep. *41*, 111655. https://doi.org/10.1016/j.celrep.2022.111655.
10. Machtinger, R., Laurent, L.C., and Baccarelli, A.A. (2016). Extracellular vesicles: roles in gamete maturation, fertilization and embryo implantation. Hum. Reprod. Update *22*, 182–193. https://doi.org/10.1093/humupd/dmv055.
11. Naz, R.K. (1998). Effect of actinomycin D and cycloheximide on human sperm function. Arch. Androl. *41*, 135–142. https://doi.org/10.3109/01485019808987955.
12. Gur, Y., and Breitbart, H. (2006). Mammalian sperm translate nuclear-encoded proteins by mitochondrial-type ribosomes. Genes Dev. *20*, 411–416. https://doi.org/10.1101/gad.367606.
13. Miller, D., and Ostermeier, G.C. (2006). Towards a better understanding of RNA carriage by ejaculate spermatozoa. Hum. Reprod. Update *12*, 757–767. https://doi.org/10.1093/humupd/dml037.
14. Zhao, C., Guo, X.J., Shi, Z.H., Wang, F.Q., Huang, X.Y., Huo, R., Zhu, H., Wang, X.R., Liu, J.Y., Zhou, Z.M., and Sha, J.H. (2009). Role of translation by mitochondrial-type ribosomes during sperm capacitation: an analysis based on a proteomic approach. Proteomics *9*, 1385–1399. https://doi.org/10.1002/pmic.200800353.
15. Rajamanickam, G.D., Kastelic, J.P., and Thundathil, J.C. (2017). Content of testis-specific isoform of Na/K-ATPase (ATP1A4) is increased during bovine sperm capacitation through translation in mitochondrial ribosomes. Cell Tissue Res. *368*, 187–200. https://doi.org/10.1007/s00441-016-2514-7.
16. Zhu, Z., Umehara, T., Okazaki, T., Goto, M., Fujita, Y., Hoque, S.A.M., Kawai, T., Zeng, W., and Shimada, M. (2019). Gene expression and protein synthesis in mitochondria enhance the duration of high-speed linear motility in boar sperm. Front. Physiol. *10*, 252. https://doi.org/10.3389/fphys.2019.00252.
17. Bisconti, M., Leroy, B., Gallagher, M.T., Senet, C., Martinet, B., Arcolia, V., Wattiez, R., Kirkman-Brown, J.C., Simon, J.F., and Hennebert, E. (2022). The ribosome inhibitor chloramphenicol induces motility deficits in human spermatozoa: a proteomic approach identifies potentially involved proteins. Front. Cell Dev. Biol. *10*, 965076. https://doi.org/10.3389/fcell.2022.965076.

18. Lahnsteiner, F. (2003). Morphology, fine structure, biochemistry, and function of the spermatic ducts in marine fish. Tissue Cell *35*, 363–373. https://doi.org/10.1016/s0040-8166(03)00057-0.

19. Forné, I., Castellana, B., Marín-Juez, R., Cerdà, J., Abián, J., and Planas, J.V. (2011). Transcriptional and proteomic profiling of flatfish (*Solea senegalensis*) spermatogenesis. Proteomics *11*, 2195–2211. https://doi.org/10.1002/pmic.201000296.

20. Groh, K.J., Nesatyy, V.J., Segner, H., Eggen, R.I.L., and Suter, M.J.F. (2011). Global proteomics analysis of testis and ovary in adult zebrafish (*Danio rerio*). Fish Physiol. Biochem. *37*, 619–647. https://doi.org/10.1007/s10695-010-9464-x.

21. Chen, J., Zhou, A., Xie, S., Wang, C., Lv, Z., and Zou, J. (2016). Comparative proteomic identification of mature and immature sperm in the catfish *Cranoglanis bouderius*. PLoS One *11*, e0151254. https://doi.org/10.1371/journal.pone.0151254.

22. Martyniuk, C.J., and Alvarez, S. (2013). Proteome analysis of the fathead minnow (*Pimephales promelas*) reproductive testes. J. Proteonomics *79*, 28–42. https://doi.org/10.1016/j.jprot.2012.11.023.

23. Dietrich, M.A., Judycka, S., Żarski, D., Malinowska, A., Świderska, B., Palińska-Żarska, K., Błażejewski, M., and Ciereszko, A. (2021). Proteomic analysis of pikeperch seminal plasma provides novel insight into the testicular development of domesticated fish stocks. Animal *15*, 100279. https://doi.org/10.1016/j.animal.2021.100279.

24. Judycka, S., Nynca, J., Hliwa, P., and Ciereszko, A. (2021). Characteristics and cryopreservation of semen of sex-reversed females of salmonid fish. Int. J. Mol. Sci. *22*, 964. https://doi.org/10.3390/ijms22020964.

25. Li, P., Hulak, M., Koubek, P., Sulc, M., Dzyuba, B., Boryshpolets, S., Rodina, M., Gela, D., Manaskova-Postlerova, P., Peknicova, J., and Linhart, O. (2010). Ice-age endurance: the effects of cryopreservation on proteins of sperm of common carp, *Cyprinus carpio* L. Theriogenology *74*, 413–423. https://doi.org/10.1016/j.theriogenology.2010.02.024.

26. Li, P., Du, H., Qiao, X.M., Liu, Z.G., Zhou, Q., and Wei Wei, Q. (2019). Protein profile of Dabry's sturgeon (*Acipenser dabryanus*) spermatozoa and relationship to sperm quality. Anim. Reprod. Sci. *201*, 1–11. https://doi.org/10.1016/j.anireprosci.2018.12.002.

27. Dietrich, M.A., Dietrich, G.J., Mostek, A., and Ciereszko, A. (2016). Motility of carp spermatozoa is associated with profound changes in the sperm proteome. J. Proteonomics *138*, 124–135. https://doi.org/10.1016/j.jprot.2016.02.029.

28. Kodzik, N., Ciereszko, A., Judycka, S., Słowińska, M., Szczepkowska, B., Świderska, B., and Dietrich, M.A. (2024). Cryoprotectant-specific alterations in the proteome of Siberian sturgeon spermatozoa induced by cryopreservation. Sci. Rep. *14*, 17707. https://doi.org/10.1038/s41598-024-68395-7.

29. Dietrich, M.A., Nynca, J., and Ciereszko, A. (2019). Proteomic and metabolomic insights into the functions of the male reproductive system in fishes. Theriogenology *132*, 182–200. https://doi.org/10.1016/j.theriogenology.2019.04.018.

30. Schulz, R.W., and Nóbrega, R.H. (2011). The reproductive organs and processes. Anatomy and histology of fish testis. In Encyclopedia of Fish Physiology, A.P. Farrell, ed. (Elsevier), pp. 616–626. https://doi.org/10.1016/b978-0-12-374553-8.00246-x.

31. Castro-Arnau, J., Chauvigné, F., Gómez-Garrido, J., Esteve-Codina, A., Dabad, M., Alioto, T., Finn, R.N., and Cerdà, J. (2022). Developmental RNA-seq transcriptomics of haploid germ cells and spermatozoa uncovers novel pathways associated with teleost spermiogenesis. Sci. Rep. *12*, 14162. https://doi.org/10.1038/s41598-022-18422-2.

32. Binns, D., Dimmer, E., Huntley, R., Barrell, D., O'Donovan, C., and Apweiler, R. (2009). QuickGO: a web-based tool for Gene Ontology searching. Bioinformatics *25*, 3045–3046. https://doi.org/10.1093/bioinformatics/btp536.

33. Thomas, P.D., Ebert, D., Muruganujan, A., Mushayahama, T., Albou, L.P., and Mi, H. (2022). PANTHER: making genome-scale phylogenetics accessible to all. Protein Sci. *31*, 8–22. https://doi.org/10.1002/pro.4218.

34. Taverner, T., Karpievitch, Y.V., Polpitiya, A.D., Brown, J.N., Dabney, A.R., Anderson, G.A., and Smith, R.D. (2012). DanteR: an extensible R-based tool for quantitative analysis of -omics data. Bioinformatics *28*, 2404–2406. https://doi.org/10.1093/bioinformatics/bts449.

35. Schwämmle, V., and Jensen, O.N. (2018). VSClust: feature-based variance-sensitive clustering of omics data. Bioinformatics *34*, 2965–2972. https://doi.org/10.1093/bioinformatics/bty224.

36. Fujita, A., Nakamura, K., Kato, T., Watanabe, N., Ishizaki, T., Kimura, K., Mizoguchi, A., and Narumiya, S. (2000). Ropporin, a sperm-specific binding protein of rhophilin, that is localized in the fibrous sheath of sperm flagella. J. Cell Sci. *113*, 103–112. https://doi.org/10.1242/jcs.113.1.103.

37. Szklarczyk, D., Gable, A.L., Nastou, K.C., Lyon, D., Kirsch, R., Pyysalo, S., Doncheva, N.T., Legeay, M., Fang, T., Bork, P., et al. (2021). The STRING database in 2021: customizable protein–protein networks, and functional characterization of user-uploaded gene/measurement sets. Nucleic Acids Res. *49*, D605–D612. https://doi.org/10.1093/nar/gkaa1074.

38. Gillespie, M., Jassal, B., Stephan, R., Milacic, M., Rothfels, K., Senff-Ribeiro, A., Griss, J., Sevilla, C., Matthews, L., Gong, C., et al. (2022). The reactome pathway knowledgebase 2022. Nucleic Acids Res. *50*, D687–D692. https://doi.org/10.1093/nar/gkab1028.

39. Chauvigné, F., Castro-Arnau, J., López-Fortún, N., Sánchez-Chardi, A., Rützler, M., Calamita, G., Finn, R.N., and Cerdà, J. (2024). Aquaporin-3a dysfunction impairs osmoadaptation in post-activated marine fish spermatozoa. Int. J. Mol. Sci. *25*, 9604. https://doi.org/10.3390/ijms25179604.

40. Dai, P., Wang, X., Gou, L.T., Li, Z.T., Wen, Z., Chen, Z.G., Hua, M.M., Zhong, A., Wang, L., Su, H., et al. (2019). A translation-activating function of MIWI/piRNA during mouse spermiogenesis. Cell *179*, 1566–1581.e16. https://doi.org/10.1016/j.cell.2019.11.022.

41. Inaba, K., Morisawa, S., and Morisawa, M. (1998). Proteasomes regulate the motility of salmonid fish sperm through modulation of cAMP-dependent phosphorylation of an outer arm dynein light chain. J. Cell Sci. *111*, 1105–1115. https://doi.org/10.1242/jcs.111.8.1105.

42. Mochida, K., Matsubara, T., Kudo, H., Andoh, T., Ueda, H., Adachi, S., and Yamauchi, K. (2002). Molecular cloning and immunohistochemical localization of ubiquitin C-terminal hydrolase expressed in testis of a teleost, the Nile Tilapia, *Oreochromis niloticus*. J. Exp. Zool. *293*, 368–383. https://doi.org/10.1002/jez.10136.

43. Pizarro, E., Pastén, C., Kong, M., and Morales, P. (2004). Proteasomal activity in mammalian spermatozoa. Mol. Reprod. Dev. *69*, 87–93. https://doi.org/10.1002/mrd.20152.

44. Dun, M.D., Aitken, R.J., and Nixon, B. (2012). The role of molecular chaperones in spermatogenesis and the post-testicular maturation of mammalian spermatozoa. Hum. Reprod. Update *18*, 420–435. https://doi.org/10.1093/humupd/dms009.

45. Hou, C.C., and Yang, W.X. (2013). New insights to the ubiquitin-proteasome pathway (UPP) mechanism during spermatogenesis. Mol. Biol. Rep. *40*, 3213–3230. https://doi.org/10.1007/s11033-012-2397-y.

46. Boryshpolets, S., Kholodnyy, V., Cosson, J., and Dzyuba, B. (2018). Fish sperm motility analysis: the central role of the flagellum. Reprod. Fertil. Dev. *30*, 833–841. https://doi.org/10.1071/RD17478.

47. Larsson, M., Norrander, J., Gräslund, S., Brundell, E., Linck, R., Ståhl, S., and Höög, C. (2000). The spatial and temporal expression of Tekt1, a mouse tektin C homologue, during spermatogenesis suggest that it is involved in the development of the sperm tail basal body and axoneme. Eur. J. Cell Biol. *79*, 718–725. https://doi.org/10.1078/0171-9335-00097.

48. Fiedler, S.E., Dudiki, T., Vijayaraghavan, S., and Carr, D.W. (2013). Loss of R2D2 proteins ROPN1 and ROPN1L causes defects in murine sperm motility, phosphorylation, and fibrous sheath integrity. Biol. Reprod. *88*, 41. https://doi.org/10.1095/biolreprod.112.105262.

49. Sapiro, R., Kostetskii, I., Olds-Clarke, P., Gerton, G.L., Radice, G.L., and Strauss III, J.F. (2002). Male infertility, impaired sperm motility, and hydrocephalus in mice deficient in sperm-associated antigen 6. Mol. Cell Biol. *22*, 6298–6305. https://doi.org/10.1128/mcb.22.17.6298-6305.2002.

50. Miyata, H., Shimada, K., Morohoshi, A., Oura, S., Matsumura, T., Xu, Z., Oyama, Y., and Ikawa, M. (2020). Testis-enriched kinesin KIF9 is important for progressive motility in mouse spermatozoa. Faseb. J. *34*, 5389–5400. https://doi.org/10.1096/fj.201902755r.

51. Lahnsteiner, F., Mansour, N., and Caberlotto, S. (2010). Composition and metabolism of carbohydrates and lipids in *Sparus aurata* semen and its relation to viability expressed as sperm motility when activated. Comp. Biochem. Physiol. *157*, 39–45. https://doi.org/10.1016/j.cbpb.2010.04.016.

52. Lahnsteiner, F., and Caberlotto, S. (2012). Motility of gilthead seabream *Sparus aurata* spermatozoa and its relation to temperature, energy metabolism and oxidative stress. Aquaculture *370*, 76–83. https://doi.org/10.1016/j.aquaculture.2012.09.034.

53. Chauvigné, F., Boj, M., Finn, R.N., and Cerdà, J. (2015). Mitochondrial aquaporin-8-mediated hydrogen peroxide transport is essential for teleost spermatozoon motility. Sci. Rep. *5*, 7789. https://doi.org/10.1038/srep07789.

54. Chauvigné, F., Ducat, C., Ferré, A., Hansen, T., Carrascal, M., Abián, J., Finn, R.N., and Cerdà, J. (2021). A multiplier peroxiporin signal transduction pathway powers piscine spermatozoa. Proc. Natl. Acad. Sci. USA *118*, e2019346118. https://doi.org/10.1073/pnas.2019346118.

55. Cappallo-Obermann, H., Schulze, W., Jastrow, H., Baukloh, V., and Spiess, A.N. (2011). Highly purified spermatozoal RNA obtained by a novel method indicates an unusual 28S/18S rRNA ratio and suggests impaired ribosome assembly. Mol. Hum. Reprod. *17*, 669–678. https://doi.org/10.1093/molehr/gar037.

56. Kerr, J.B. (1992). Functional cytology of the human testis. Baillieres Clin. Endocrinol. Metab. *6*, 235–250. https://doi.org/10.1016/s0950-351x(05)80149-1.

57. Gur, Y., and Breitbart, H. (2008). Protein synthesis in sperm: dialog between mitochondria and cytoplasm. Mol. Cell. Endocrinol. *282*, 45–55. https://doi.org/10.1016/j.mce.2007.11.015.

58. Connor, M.K., Takahashi, M., and Hood, D.A. (1996). Tissue-specific stability of nuclear- and mitochondrially encoded mRNAs. Arch. Biochem. Biophys. *333*, 103–108. https://doi.org/10.1006/abbi.1996.0369.

59. Ren, X., Chen, X., Wang, Z., and Wang, D. (2017). Is transcription in sperm stationary or dynamic? J. Reprod. Dev. *63*, 439–443. https://doi.org/10.1262/jrd.2016-093.

60. Freitas, M.J., Patrício, D., and Fardilha, M. (2020). Sperm signaling specificity: from sperm maturation to oocyte recognition. In Tissue-Specific Cell Signaling, J.V. Silva, M.J. Freitas, and M. Fardilha, eds. (Cham: Springer), pp. 257–277. https://doi.org/10.1007/978-3-030-44436-5_9.

61. Wu, S.F., Zhang, H., and Cairns, B.R. (2011). Genes for embryo development are packaged in blocks of multivalent chromatin in zebrafish sperm. Genome Res. *21*, 578–589. https://doi.org/10.1101/gr.113167.110.

62. Tan, B.C.M., Yang, C.C., Hsieh, C.L., Chou, Y.H., Zhong, C.Z., Yung, B.Y.M., and Liu, H. (2012). Epigeneitc silencing of ribosomal RNA genes by Mybbp1a. J. Biomed. Sci. *19*, 57. https://doi.org/10.1186/1423-0127-19-57.

63. Cong, R., Das, S., Ugrinova, I., Kumar, S., Mongelard, F., Wong, J., and Bouvet, P. (2012). Interaction of nucleolin with ribosomal RNA genes and its role in RNA polymerase I transcription. Nucleic Acids Res. *40*, 9441–9454. https://doi.org/10.1093/nar/gks720.

64. Jones, B., Su, H., Bhat, A., Lei, H., Bajko, J., Hevi, S., Baltus, G.A., Kadam, S., Zhai, H., Valdez, R., et al. (2008). The histone H3K79 methyltransferase dot1l is essential for mammalian development and heterochromatin structure. PLoS Genet. *4*, e1000190. https://doi.org/10.1371/journal.pgen.1000190.

65. Wood, K., Tellier, M., and Murphy, S. (2018). DOT1L and H3K79 methylation in transcription and genomic stability. Biomolecules *8*, 11. https://doi.org/10.3390/biom8010011.

66. Kurtz, K., Saperas, N., Ausió, J., and Chiva, M. (2009). Spermiogenic nuclear protein transitions and chromatin condensation. Proposal for an ancestral model of nuclear spermiogenesis. J. Exp. Zool. B Mol. Dev. Evol. *312*, 149–163. https://doi.org/10.1002/jez.b.21271.

67. Perez-Riverol, Y., Bai, J., Bandla, C., García-Seisdedos, D., Hewapathirana, S., Kamatchinathan, S., Kundu, D.J., Prakash, A., Frericks-Zipper, A., Eisenacher, M., et al. (2022). The PRIDE database resources in 2022: a hub for mass spectrometry-based proteomics evidences. Nucleic Acids Res. *50*, D543–D552. https://doi.org/10.1093/nar/gkab1038.

68. Chauvigné, F., Parhi, J., Ducat, C., Ollé, J., Finn, R.N., and Cerdà, J. (2018). The cellular localization and redistribution of multiple aquaporin paralogs in the spermatic duct epithelium of a maturing marine teleost. J. Anat. *233*, 177–192. https://doi.org/10.1111/joa.12829.

69. Chauvigné, F., Boj, M., Vilella, S., Finn, R.N., and Cerdà, J. (2013). Subcellular localization of selectively permeable aquaporins in the male germ line of a marine teleost reveals spatial redistribution in activated spermatozoa. Biol. Reprod. *89*, 37. https://doi.org/10.1095/biolreprod.113.110783.

70. Farah, O.I., Cuiling, L., Jiaojiao, W., and Huiping, Z. (2013). Use of fluorescent dyes for readily recognizing sperm damage. J. Reproduction Infertil. *14*, 120–125.

71. Wiśniewski, J.R., Zougman, A., Nagaraj, N., and Mann, M. (2009). Universal sample preparation method for proteome analysis. Nat. Methods *6*, 359–362. https://doi.org/10.1038/nmeth.1322.

STAR★METHODS

KEY RESOURCES TABLE

REAGENT or RESOURCE	SOURCE	IDENTIFIER
Antibodies		
Rabbit polyclonal anti-EEF1A1	MyBiosurce	MBS9205539; RRID: N/A
Rabbit polyclonal anti-RPS2	GeneTex	GTX114734; RRID:AB_10620358
Rabbit polyclonal anti-RPS13	MyBiosurce	MBS8242294; RRID: N/A
Rabbit polyclonal anti-RPL31	GeneTex	GTX129792; RRID:AB_2886091
Rabbit polyclonal anti-MRPS5	MyBiosurce	MBS3218645; RRID: N/A
Rabbit polyclonal anti-MRPL28	MyBiosurce	MBS3210650; RRID: N/A
Rabbit polyclonal anti-DNAI2	MyBiosurce	MBS3206467; RRID: N/A
Mouse monoclonal anti-Tuba	Sigma-Aldrich	T9026; RRID:AB_477593
Rabbit polyclonal anti-SPAG6	MyBiosurce	MBS3211442; RRID: N/A
Rabbit polyclonal anti-DYNLL2	Affinity Biosciences	DF12966; RRID:AB_2845927
Rabbit polyclonal anti-HSP90	GeneTex	GTX101448; RRID:AB_1950515
Rabbit polyclonal anti-seabream Aqp3a	Custom made[68]	N/A
Rabbit polyclonal anti-BODIPY FL	Invitrogen; ThermoFisher Scientific	A-5770; RRID: N/A
Rabbit polyclonal anti-PHB	Genetex	GTX124491; RRID:AB_11169327
Goat anti-rabbit IgG (H+L) HRP conjugate	BioRad	172-1019; RRID: N/A
Goat anti-mouse IgG (H+L)-HRP conjugate	BioRad	172-1011; RRID: N/A
Sheep anti-rabbit IgG (whole molecule), F(ab)2 fragment-Cy3	Sigma-Aldrich	C2306; RRID:AB_258792
Mouse IgG Alexa Fluor 555	Invitrogen; ThermoFisher Scientific	A28180; RRID: N/A
Biological samples		
Gilthead seabream (*Sparus aurata*) testis	Collected from captive-raised commercial fish (Avramar España Acuicultura, Spain)	N/A
Gilthead seabream (*Sparus aurata*) spermatozoa from efferent duct	Collected from captive-raised commercial fish (Avramar España Acuicultura, Spain)	N/A
Gilthead seabream (*Sparus aurata*) ejaculated spermatozoa	Collected from captive-raised commercial fish (Avramar España Acuicultura, Spain)	N/A
Chemicals, peptides, and recombinant proteins		
Actinomycin D	Sigma-Aldrich	A9415; CAS: 50-76-0
Chloramphenicol	Sigma-Aldrich	C1919; CAS: 56-75-7
Cycloheximide	Sigma-Aldrich	C7698; CAS: 66-81-9
Wheat Germ Agglutinin (WGA) Alexa Fluor® 647 conjugate	Invitrogen; ThermoFisher Scientific	W32466: N/A
MitoTracker® Red CMXRos dye	Invitrogen; ThermoFisher Scientific	M46752; CAS: N/A
Critical commercial assays		
TRIzol reagent	Invitrogen; ThermoFisher Scientific	15596026
FluoroTect™ GreenLys *in vitro* Translation Labeling System	Promega	L5001
SUPERase In Rnase inhibitor	Invitrogen; ThermoFisher Scientific	AM2696
RNasin® Plus Ribonuclease Inhibitor	Promega	N2611
TURBO DNase	Invitrogen; ThermoFisher Scientific	AM2238
WesternSure® PREMIUM chemiluminescent substrate	LI-COR	926-95000
RNA 6000 Pico Kit for 2100 Bioanalyzer Systems	Agilent Technologies	5067-1513

(*Continued on next page*)

Continued

REAGENT or RESOURCE	SOURCE	IDENTIFIER
Deposited data		
Mass spectrometry proteomic data	This study	ProteomeXchange Consortium via the PRIDE[67] partner repository. Project ID: PXD056370
Experimental models: Organisms/strains		
Gilthead seabream (*Sparus aurata*) F1 generation	Avramar (España Acuicultura, Spain) commercial fish farm ()	N/A
Oligonucleotides		
Primers used in this study are listed in Table S10	This study	N/A
Software and algorithms		
Integrated Semen Analysis (ISAS®v1)	Proisier, Valencia, Spain	N/A
Proteome Discoverer v1.4 (6-plex TMT)	ThermoFisher Scientific	RRID:SCR_014477; https://www.thermofisher.com/order/catalog/product/IQLAAEGABSFAKJMAUH
Proteome Discoverer v2.5 (10-plex TMT)	ThermoFisher Scientific	RRID:SCR_014477; https://www.thermofisher.com/order/catalog/product/IQLAAEGABSFAKJMAUH
Uniprot	Uniprot	RRID:SCR_002380 https://www.uniprot.org
DanteR	Taverner et al.[34]	RRID: N/A; http://omics.pnl.gov/software/danter
VSClust	Schwämmle and Jensen[35]	RRID: N/A; http://computproteomics.bmb.sdu.dk/Apps/VSClust
QuickGo	EMBL-EBI	RRID:SCR_004608; https://www.ebi.ac.uk/QuickGO
PANTHER classification system	PANTHER knowledgebase	RRID:SCR_004869; http://www.pantherdb.org
Rstudio v2022.12.0+353	Rstudio	RRID:SCR_000432; http://www.rstudio.com
GraphPad Prism v10.3.1	GraphPad Prism	RRID:SCR_002798 http://www.graphpad.com
STRING database v11.5	STRING Consortium	RRID:SCR_005223; https://string-db.org
Cytoscape v3.9.1	Cytoscape	RRID:SCR_003032 https://cytoscape.org
Reactome	Reactome	RRID:SCR_003485; http://www.reactome.org
Image Studio 5.2	LI-COR	RRID:SCR_015795; https://www.licor.com/bio/image-studio
CytExpert v2.6	Beckman Coulter	RRID:SCR_017217; https://www.beckman.fr/flow-cytometry/instruments/cytoflex/software
Agilent Bioanalyzer 2100 Expert Software	Agilent Technologies	RRID:SCR_019715; https://www.agilent.com/cs/library/posters/Public/BioAnalyzer.PDF

EXPERIMENTAL MODEL AND STUDY PARTICIPANT DETAILS

Juvenile gilthead seabream (*Sparus aurata*) F1 generation were obtained from a commercial fish farm (Avramar España Acuicultura, Spain) and raised up to the age of 2-3 years as described previously.[69] During the natural reproductive season (November-February), males were anaesthetised with 100 ppm 2-phenoxyethanol and samples of SPZ_{EJ} were collected from males by abdominal massage as described previously.[31] The fish were subsequently euthanized and SPZ_{ED} were extracted with a micropipette after an incision in the dorsal and anterior region of the testis. Procedures relating to the care and use of animals and sample collection were approved by the Ethics Committee of the Spanish National Research Council (CSIC) and the Department of Climate Action, Food and Rural Agenda, General Directorate of Environmental Policies and the Natural Environment (Government of Catalonia) (project no. 12147).

METHOD DETAILS

Sperm motility assays

Freshly collected SPZ_{IT}, SPZ_{ED} and SPZ_{EJ} were diluted 1:100 in NAM (in mg/ml: NaCl 3.5, KCl 0.11, $MgCl_2$ 1.23, $CaCl_2$ 0.39, $NaHCO_3$ 1.68, glucose 0.08, and 0.2% bovine serum albumin, pH 7.8, 270-290 mOsm), and their concentration and kinematic properties after seawater activation determined by CASA using the ISAS®v1 software as described previously.[31,69] For some experiments, SPZ_{EJ} ($\sim 10^8$ cells) were incubated in NAM at 16°C in a temperature-controlled incubator up to 13 h, in the presence of 100 μg/ml of the inhibitors CHX or CP, or the drugs vehicle (0.5% ethanol), before sperm motility was activated and evaluated. In these experiments, the viability of spermatozoa after the incubation time was assessed by treating the cells with 250 ng/ml of the mitochondria-selective

cationic dye MitoTracker® Red CMXRos[70] for 15 min at room temperature, and further calculation of the percentage of spermatozoa showing red fluorescence within the mitochondria (viable cells) using the Vitality Module of the CASA system.

Sample preparation for LC-MS/MS quantitative proteomics

Populations of HGC and SPZ_{IT} were isolated by FACS from freshly collected testis biopsies as described previously,[31] and aliquots of 3-5 × 10^6 cells were frozen in liquid nitrogen and stored at -80°C. Aliquots of SPZ_{ED} and SPZ_{EJ} (both containing 10^9 cells) were frozen as above. To isolate nuclear fraction-enriched sperm samples, SPZ_{ED} and SPZ_{EJ} were resuspended in 1.2 ml of nuclei buffer, containing 0.25 M sucrose, 5 mM $CaCl_2$, 10 Mm Tris HCl pH 7.4, 10 mM benzamidine chloride, 1 mM NaF, 1 mM Na_3V0_4, protease inhibitors (Sigma-Aldrich, 11836170001), and homogenized in a Dounce homogenizer on ice. The homogenate was centrifuged at 2,000 × *g* for 10 min at 4°C, and the pellets containing the nuclei homogenized in the nuclei buffer supplemented with 0.5% Triton X-100 and incubated for 15 min on ice. The homogenate was centrifuged again and the resulting pellets were washed twice in the nuclei buffer. The final nuclear pellet was frozen in liquid nitrogen and stored at -80°C.

Sperm samples were lysed in 4.4% sodium dedocylsulfate (SDS), 0.1 M Tris and incubated in a Thermomixer at 300 rpm for 15 min at 15°C. For each cell type, three pools (biological replicates) of five different males each, or five biological replicates, each replicate representing one different male, were prepared. Individual or pooled samples were sonicated (5 x 1 s, 40% power) and centrifuged at 16,000 × *g* for 10 min at 15°C. The sonication and centrifugation process was repeated once. The protein concentration was determined following the bicinchoninic acid (BCA) method. Then, 1 M dithiothreitol (DTT) was added to each sample to reach a final concentration of 100 mM, incubated 5 min at 95°C with 600 rpm in a Thermomixer, and centrifuged at 16,000 × *g* for 15 min at 15°C.

Protein digestion, isobaric labeling and fractionation

Fifty μg (6-plex TMT for whole cell extracts) or 80 μg (10-plex TMT for nuclear extracts) of protein from each sample were digested according to the FASP digestion method[71] for 16-18 h at 37°C. Briefly, samples were diluted in UA buffer (8 M urea 100 mM Tris-HCl pH 8.5) and loaded onto 10 kDa centrifugal filter devices (Millipore). After washing the filters, the UA proteins were alkylated with iodoacetamide for 20 min in the dark. The excess alkylating reagent was removed by consecutive washes with UA buffer and triethylammonium bicarbonate (TEAB). Proteins were digested overnight at 37°C with 3% ratio (w/w) of modified trypsin (Promega). The resulting peptides were eluted in 20 mM TEAB and dried for further analysis.

For isobaric labelling, the tryptic peptides were processed for two sets of 6-plex TMT labelling or one set of 10-plex TMT (Fisher scientific). Dried samples were reconstituted in 20 mM TEAB and labelled using TMT reagents previously reconstituted in acetonitrile following the manufacturer's protocol. After incubation at room temperature for 1 h, the reaction was stopped by incubating the plex samples for 15 min with 5% of hydroxylamine and the peptides were combined. The samples were again dried to desalt the peptides using PolyLC C18 tips (Fisher scientific).

The TMT-labelled samples were fractionated by strong cation exchange (SCX) (6-plex TMT) or High-pH-Reverse phase (HP-RP) (10-plex TMT). The SCX was performed in a HPLC 1100 UV-Vis apparatus (Agilent) with a Polysulfoehtyl A TM, 200 x 2.1 mm, 5 μm, 200A (PolyLC). Peptides were eluted with a continuous salt gradient of 3-70% Solvent B (A: 70% H2O Milli-Q, 30% acetonitrile [ACN], 0.1% formic acid; B: 70% H2O Milli-Q, 500 mM NH4Cl, 30% ACN, 0.1% formic acid [FA]) at a flow rate of 200 μl/min. The HP-RP was performed in a HPLC 1100 UV-Vis (Agilent), with a XBridge Peptide BEH C18, 130Å, 5 μm, 2.1 mm x 100 mm column (Waters, 186003575). Peptides were eluted with a gradient from 3-60% Solvent B (A: 5 mM ammonium formate, pH 10, 2% CAN; B: 5 mM ammonium formate, pH 10, 90% ACN) at a flow rate of 200 μl/min. All the fractions that were obtained for each experiment were mixed, obtaining a final number of 5 fraction mixes for the 6-plex TMT and 6 for the 10-plex TMT.

LC-MS/MS analysis

Samples from the 6-plex TMT were injected into a chromatographic system equipped with a C18 preconcentration column (300 μm id x 0.5 cm, Agilent Technologies) and an analytical column (100 μm id x 15 cm, Nikkyo Technos Co). Peptides were loaded onto the preconcentration column using 1% FA as a solvent. Peptides were eluted directly to the analytical column at a flow rate of 400 nl/min using a 0-40% ACN (0.1% FA) gradient in 120 min. The chromatographic system was connected on-line to a high-resolution LTQ-Orbitrap XL mass spectrometer (ThermoFisher Scientific), performing the analysis in dependent scan mode: a full scan (m/z range 400-1800) using the Orbitrap with a resolution of 60,000 and 10 parallel scans of MS/ MS (5 in CID mode and 5 in HCD mode) on the most abundant precursors.

For the analysis of the 10-plex TMT the MS system used was a Fusion Lumos™ Tribrid mass spectrometer coupled to a Thermo Scientific Dionex Ultimate 3000 chromatographic system (ThermoFisher Scientific). Samples were loaded into a Acclaim PepMap100 C18 Trap column (100 μm × 2 cm, 5 μm, 100 Å; Thermo Scientific) at 15 μl/min, connected to a NanoEase MZ HSS T3 column (75 μm × 250 cm, 1.8 μm, 100 Å; Waters). The separation was done at 250 nl/min, gradient 3-35% ACN (0.1% FA) in 60 min. The end of the chromatographic column was directly connected to an Advion TriVersa NanoMate system coupled to the spectrometer and working at 1.7 kV. The spectrometric analysis was performed in a data dependent mode, m/z range 375-1500, SPS3 fragmentation, Top speed method with a collision energy of 35% for MS2 CID and 65% for MS3 HCD. The detection was done in the Orbitrap (MS1 120k), Ion trap (MS2) and Orbitrap (MS3 60 kDa).

Immunofluorescence microscopy and immunoblotting

Immunofluorescence microscopy was carried out as described previously,[31] except that in some cases the sperm mitochondrion was labelled by incubating live spermatozoa with 250 ng/ml of the mitochondria-specific vital dye MitoTracker Green FM for 15 min prior to fixation. The immunoblotting procedures were also as described previously,[69] but in this case intact samples of SPZ_{ED} and SPZ_{EJ} were homogenized in 500 μl 1 × Laemmli sample buffer with 10 μl benzonase and sonicated for 30 s at 20% amplitude using a Digital Sonifier® S250D (Branson Ultrasonics Corp.), for protein extraction. The dilutions of the primary and secondary antibodies employed for immunostaining and immunoblotting are listed in Table S9. Immunoreactive bands obtained in Western blot were revealed by the WesternSure® PREMIUM Chemiluminescent Substrate (LI-COR) using a digital scanner (C-DiGit® Blot Scanner, LI-COR). For quantitation of protein abundance, the intensity of the corresponding immunoreactive bands was determined by densitometry using the software Image Studio 5.2 (LI-COR) and normalized to that of Phb or H3.

Protein labelling by $tRNA^{Lys}$ tagged with BODIPY®-FL

Samples of freshly collected SPZ_{ED} or SPZ_{EJ} diluted in NAM (5×10^9 cells/ml) were partially permeabilized with 0.02% Triton X-100 for 30 s, and further diluted 10 times in NAM with 0.5% BSA (5×10^8 cells/ml). The absence of contamination by somatic cells or HCG in the SPZ_{ED} and SPZ_{EJ} cell fractions was confirmed by fluorescence microscopy employing the wheat germ agglutinin (WGA) lectin as well as by flow cytometry using a CytoFLEX cytometer (Beckman Coulter Life Sciences). An aliquot of 100 μl of SPZ_{ED} (5×10^7 cells) was incubated at different times (1 s, or 2, 6 and 20 h) in the presence of 3 μl of $tRNA^{Lys}$-BODIPY®-FL from the FluoroTect™ $Green_{Lys}$, *in vitro* translation system at 16°C in a temperature-controlled incubator. The negative controls were incubated without $tRNA^{Lys}$-BODIPY for 20 h. After the incubation time, sperm motility was analyzed with CASA to assure that the viability of spermatozoa was not affected. In some experiments, SPZ_{ED} were incubated with $tRNA^{Lys}$-BODIPY in the presence of 100 μg/ml of the inhibitors ActD, CHX or CP, or the drug vehicles (0.5% dimethyl sulfoxide [DMSO] or 0.5% ethanol). Subsequently, samples were homogenized with 4 × Laemmli sample buffer and processed for immunoblotting as described above using a rabbit polyclonal BODIPY®-FL primary antibody, and the PhB antibody to verify equal loading (Table S9).

Sucrose density gradient fractionation of spermatozoa

The RNA size distribution profiles of HGC, SPZ_{ED} and SPZ_{EJ} (10^7 cells) were analyzed using the Agilent 2100 Bioanalyzer (Agilent Technologies). For sperm fractionation, frozen SPZ_{ED} samples (10^9 cells) were homogenized in 500 μl of lysis buffer (20 mM Tris-HCl pH 7.5, 100 mM NaCl, 10 mM $MgCl_2$, 1 % Triton X-100, 0.5 % sodium deoxycholate, 1 mM dithiothreitol, 200 μg/ml CHX, 10 U SUPERase·In RNase inhibitor, 20 U RNasin plus RNase inhibitor, 21 U TURBO DNase, and cOmplete EDTA-free protease inhibitor cocktail (Roche, 11873580001). The extracts from two samples were combined into one tube which was incubated for 5 min at 4°C under continuous rotation (60 rpm). The sample was then passed through a 23G needle 10 times, and through a 26G needle another 5 times, and incubated again for 30-45 min at 4°C under continuous rotation (60 rpm). Lysates were clarified by centrifugation at 8,000 × *g* for 5 min at 4°C. An aliquot of the clarified lysate (700 μl) was loaded onto 10-50 % sucrose density, home-made gradients in open-top polyclear centrifuge tubes (Seton Scientific). Tubes were centrifuged at 210,100 × *g* for 3 h at 4°C (SW-41 Ti rotor, Beckmann Coulter ultracentrifuge). Samples were fractionated using a Piston Gradient Fractionator (Biocomp Instruments) at 0.75 ml/min and absorbance recorded at A260. Thirty fractions of 0.37 ml each were collected in 1.5 ml tubes, flash frozen, and stored at -80°C. The RNA and protein from each sample were purified using 1.5 ml TRIzol to which 300 μl of chloroform was added before centrifugation at 12,000 × *g* for 15 min at 4°C. The aqueous phase was processed for RNA extraction, while the organic and interphase phases were processed for protein extraction following the manufacturer's instructions. For both RNA and protein, the 30 collected fractions were pooled into 10 samples. The samples were analysed by RT-PCR using specific oligonucleotides (Table S10) as described previously,[69] as well as by immunoblotting as indicated above. Alternatively, pooled samples were directly precipitated by trichloroacetic acid (TCA) by adding 1 volume of TCA to 5 volumes of sample. After vortexing, proteins were allowed to precipitate o/n at -20°C and the following day centrifuged at 14,000 × *g* for 15 min at 4°C. The protein pellet was washed twice with 200 μl cold 95 % acetone, subsequently dried for 15 min, and finally resuspended in 1 × Laemmli sample buffer for immunoblotting analysis.

QUANTIFICATION AND STATISTICAL ANALYSES

Protein identification and quantitation by proteomic analysis

The identification of the peptides in the database was carried out using the Proteome Discoverer v1.4 (6-plex TMT) or v2.5 (10-plex TMT) software from Thermo-Instruments using a previously published seabream RNA-seq database.[31] Searches were run against targeted and decoy databases, and the search parameters included: trypsin enzyme specificity, allowing for two missed cleavage sites, carbamidomethyl in cysteine TMT in lysine and in peptide N-term as static modifications, and oxidation in methionine and acetyl in the protein N-terminal as dynamic modifications. Peptide mass tolerance was 20 ppm (6-plex TMT) or 10 ppm (10-plex TMT) and the MS/MS tolerance was 0.02 Da (6-plex TMT and 10-plex TMT). Peptide identification was filtered using the percolator node at a false discovery rate (FDR) of 1 % based on the number of hits against the reversed sequence database.

The quantification of the proteins was carried out based on the intensity of the reporter ions derived from the TMT labelling and only unique peptides (peptides that only belong to one protein) were taken into account. Within each TMT experiment, peptide

quantification was normalized by summing the abundance values for each channel over all the peptides identified within an experiment. Principal components analysis (PCA) was performed to detect and visualize the variation in sperm proteins among the experimental groups by using the DanteR software, and 2D main principal components were plotted. All the proteins identified among HGC, SPZ_{IT} and SPZ_{EJ} were clustered by using VSClust software[35] considering minimum membership value >0.5. After confirming the PCA results, protein quantification was achieved by summing all the normalized peptide intensities for a given protein. The proteome data were first transformed to a log scale to apply a linear model, and the statistical analysis to determine differentially accumulated proteins was performed using the DanteR software. Differentially expressed proteins were filtered by an average cut-off change of 1.15-fold and $P < 0.05$.

Protein functional classification and pathway analyses

The GO enrichment analysis was carried out with the UniProt-IDs of identified proteins retrieved from UniProt database, using the QuickGO browser and Panther classification system v17. Classification of proteins into functional and cellular localization categories was carried out manually using QuickGO and Uniprot. Pie charts and heatmaps were plotted with 'plotrix' v3.8-2 R and 'pheatmap' R v1.0.12 packages, respectively, from Rstudio v2022.12.0+353, while volcano plots and bar plots were generated using the GraphPad Prism v10.3.1 software. Interactome analyses were conducted using the STRING database v11.5 selecting *S. aurata* as organism and with a high confidence interaction score of 0.7, and plots were performed using Cytoscape v3.9.1. Reactome pathways of differentially expressed proteins between SPZ_{ED} and SPZ_{EJ} were mapped using Panther and the Reactome database. The protein sets with an FDR q-value <0.05 and ≥ 4 members were considered over-represented. Over-represented pathways with similar biological functions and identical protein contributions (i.e., redundant results) were collapsed into a single annotation, and the non-redundant pathways with a z-score ±2 were then visualized.

Statistical analyses of sperm kinetic parameters and semiquantitative western blot

Data on sperm motility and semiquantitative immunoblotting were statistically analyzed by the two-tailed unpaired Student's *t*-test, or by the nonparametric Mann Whitney test when variances were not equal, or by one-way ANOVA followed by the Dunnett's multiple comparisons test. Percentages were square root transformed prior to analyses. Statistical analyses were carried out using GraphPad Prism v10.3.1. In all cases, statistical significance was defined as $P < 0.05$.